Recombinase system-dependent copackaging strategy for highly efficient neurocircuit tracing

Pei Sun[1,3,7], Sen Jin[2,4,7], Sijue Tao[1,2,3,7], Junjun Wang[1,3], Anan Li[1,3], Ning Li[1,3], Yang Wu[2], Jianxia Kuang[1,3], Yurong Liu[1,3], Lizhao Wang[6], Huimin Lin[1,3] Xiaohua Lv[1,3], Xiuli Liu[1,3], Jundan Peng[2], Siyu Zhang[6], Min Xu[5], Zhen Luo[2], Xiaobin He[2], Xiangning Li[1,3], Shaoqun Zeng[1,3], Yu-Hui Zhang[1,3] and Fuqiang Xu[1,2,3,7*]

[1]Britton Chance Center for Biomedical Photonics, Wuhan National Laboratory for Optoelectronics-Huazhong University of Science and Technology, Wuhan, Hubei 430074, China

[2]Centre for Brain Science, State Key Laboratory of Magnetic Resonance and Atomic Molecular Physics, Key Laboratory of Magnetic Resonance in Biological Systems, Wuhan Institute of Physics and Mathematics, CAS Centre for Excellence in Brain Science and Intelligence Technology, Chinese Academy of Sciences, Wuhan 430071, China.

[3]MoE Key Laboratory for Biomedical Photonics, School of Engineering Sciences, Huazhong University of Science and Technology, Wuhan, Hubei 430074, China

[4]HUST-Suzhou Institute for Brainsmatics, JITRI Institute for Brainsmatics, Suzhou 215215, China.

[5]Institute of Neuroscience, CAS Center for Excellence in Brain Science and Intelligence Technology, Chinese Academy of Sciences, 200031, Shanghai, China.

[6]Department of Anatomy and Physiology, Shanghai Jiao Tong University School of Medicine, 200025, Shanghai, China.

[7]These authors contributed equally to this work.

Correspondence should be addressed to Y.-H. Z (email: zhangyh@mail.hust.edu.cn) or F. X. (email: fuqiang.xu@wipm.ac.cn)

ABSTRACT

Despite significant progresses in dissecting neural circuits with recombinant adeno-associated viruses (rAAVs), compatible and efficient gene expressions of multiple vectors within the same cell still remains challenging. Here, we developed MAP-ENVIVIDERS, a recombinase system-dependent (including Cre-lox/Flp-FRT

recombinase systems) viral copackaging strategy to ameliorate mutual suppression and enhance compatibility among different rAAVs to improve neurocircuit tracing. For neuron labeling with wild-type and Cre-driver line mice, MAP-ENVIVIDERS was ~5-fold and over 10-fold more sensitive than the mixture of independently packaged rAAVs, respectively, enabling us to identify new type of neurons and capture massive morphological details of individual neurons (for example, a cholinergic neuron with 9,500+ axonal branches). For trans-monosynaptic retrograde tracing with rabies virus-mediated systems, MAP-ENVIVIDERS achieved 10- to 70-fold enhancement of tracing efficiency in 40% of all input brain regions compared with the previous strategies. Therefore, MAP-ENVIVIDERS provides powerful tools for elucidating morphological detail and organization of neurocircuits.

INTRODUCTION

Multiple rAAVs are extensively involved in basic and clinical researches where co-expression of multiple genes is needed[1]. In neural circuit studies, multiple rAAVs-mediated systems have been broadly used for brain-wide mapping of long-range projections[2-5], tracing of direct input networks[6-11] and manipulating and monitoring of neuronal activities during/for specific behaviour[12-13].

In previous strategies, these systems that required simultaneous gene expression of two or more genes were generally delivered by co-injecting mixtures of different independently packaged rAAVs. A remarkable example that uses combinations of rAAVs is the most broadly used rabies virus (RV)-mediated trans-monosynaptic systems for tracing the direct input network of a given type of neuron. Besides genetically modified glycoprotein-deleted RV (RV*dG*), this system generally used at least two Cre-dependent rAAVs with one of them to express receptor TVA, which allows entry of RV into the cells through the TVA-envelope protein from avian ASLV type A (EnvA) interaction and the other to express glycoprotein (RG) for the assembly of infectious RV[6-9]. Although great achievements have been achieved in enhancing efficiency of rAAVs[14-16], including engineering of promoters and enhancers and optimization of the protein capsid for desired tropism, problems such as low expression levels with large unpredictability for different genes in a given neuron still hinder efficient characterization of neurocircuits. For instance, with the current RV-mediated trans-monosynaptic tracing systems, the values of the total input over the total starter cells remained rather low and varied greatly among different experimental animals[5,8,9,17,18]. These problems might be deprived from the process of packaging different rAAVs as well as the innate interaction among different rAAVs. The components and impurities of each independently packaged rAAVs, which are generated from their own host cells and separate preparation procedures, but crucial for their infection efficiency[19-21], can be rather different. Mutual suppression is prevalent among different types of viruses, e.g., AAV over herpes simplex virus[22], AAV over adenovirus[23], or even among the same types of viruses (e.g., herpes simplex virus and pseudorabies virus)[24-26]. Therefore, we hypothesized that interaction between different rAAVs, though have rarely been examined, will significantly affect the expression level and the ratio among different genes in a given cell.

Herein, we first demonstrated the existence of strong mutual suppression between recombinant serotype 9 AAVs and then illustrated that copackaging the corresponding rAAV-producing plasmids significantly ameliorated this suppression and enhanced compatibility of gene expressions of multiple vectors within the same cell. Subsequently, we utilized recombinase system (including Cre-lox/Flp-FRT recombinase systems) along with viral copackaging strategy for further amplification of this compatibility and developed the MAP-ENVIVIDERS (**m**ultifaceted **a**melioration **p**rocess to **e**nhance **n**eurocircuit **vi**sualization by **vi**ral vectors **de**pending on **r**ecombinase **s**ystems) strategy to improve circuit tracing. MAP-ENVIVIDERS exhibited great advantages in complicated systems requiring co-expression of multiple rAAVs. For instance, when applied for neuron labeling with wild-type and Cre-driver line mice, MAP-ENVIVIDERS was ~5-fold and over 10-fold more sensitive than the mixture of independently packaged rAAVs. When applied for trans-monosynaptic retrograde tracing with RV-mediated systems, MAP-ENVIVIDERS improved the tracing efficiency throughout the brain, with a 10- to 70-fold increase in 40% of all input brain regions compared with the previous strategies. MAP-ENVIVIDERS is promising to serve as a powerful and versatile tool to further our understanding of the organization of neural circuits.

RESULTS

Copackaging of rAAVs significantly reduces their mutual suppression

In order to faithfully evaluate the degree of interaction between two highly similar rAAVs, we used two independently packaged, same serotyped rAAVs (rAAV2/9) under the control of a ubiquitous promoter (EF1α) but expressing different fluorescent proteins (EYFP or mCherry) and injected equal ratio mixture (abbreviated for sAAV-EYFP/mCherry for convenience, s refers to stranger hereafter) into the primary motor cortex (MOp) of wild-type mice. For the controls, a parallel procedure was followed but with rAAV2/9-EYFP or rAAV2/9-mCherry mixed equally with phosphate-buffered saline (PBS). The fluorescence intensity[27] was significantly lower for both EYFP and mCherry when the vectors were used in combination than when used separately (**Fig. 1a**,**b**), by a factor of 2.4 for EYFP and 1.4 for mCherry (**Fig. 1c**), demonstrating significant mutual suppression among different rAAVs.

Several previous studies have employed viral copackaging strategy for cost- and time-effective AAV manufacturing[28,29], we next examined whether this strategy could increase homogeneity over independently packaged rAAVs. To achieve this, we copackaged the two corresponding plasmids at a 1:1 ratio and then injected the resulting rAAVs (abbreviated as lAAV-EYFP/mCherry, where l refers to littermate hereafter) into MOp as described above. Equivalent expressions of EYFP and mCherry within individual cells were observed more frequently in neurons co-infected by lAAV-EYFP/mCherry than in neurons coinfected by sAAV-EYFP/mCherry, which instead tended to produce unbalanced expression of EYFP and mCherry (**Fig. 1d**,**e**, top vs. bottom rows). For neurons with unbalanced expressions (arrows in **Fig. 1e**), the ratio of mCherry/EYFP and EYFP/mCherry fluorescence intensity with higher mCherry and EYFP signals, respectively, was significantly higher in neurons injected with sAAV-EYFP/mCherry than in those injected with lAAV-EYFP/mCherry (mCherry/EYFP ratio (pink arrows): 3.44 ± 0.76 vs. 1.46 ± 0.20, respectively, and EYFP/mCherry ratio (cyan arrows): 2.50 ± 0.37 vs. 1.48 ± 0.12, respectively; mean ± s.e.m, unpaired t-test, $P < 0.0001$, $n = 3$ mice, **Fig. 1f**). These results indicated that copackaging rAAVs can substantially reduce mutual suppression and significantly enhance compatibility among different rAAVs.

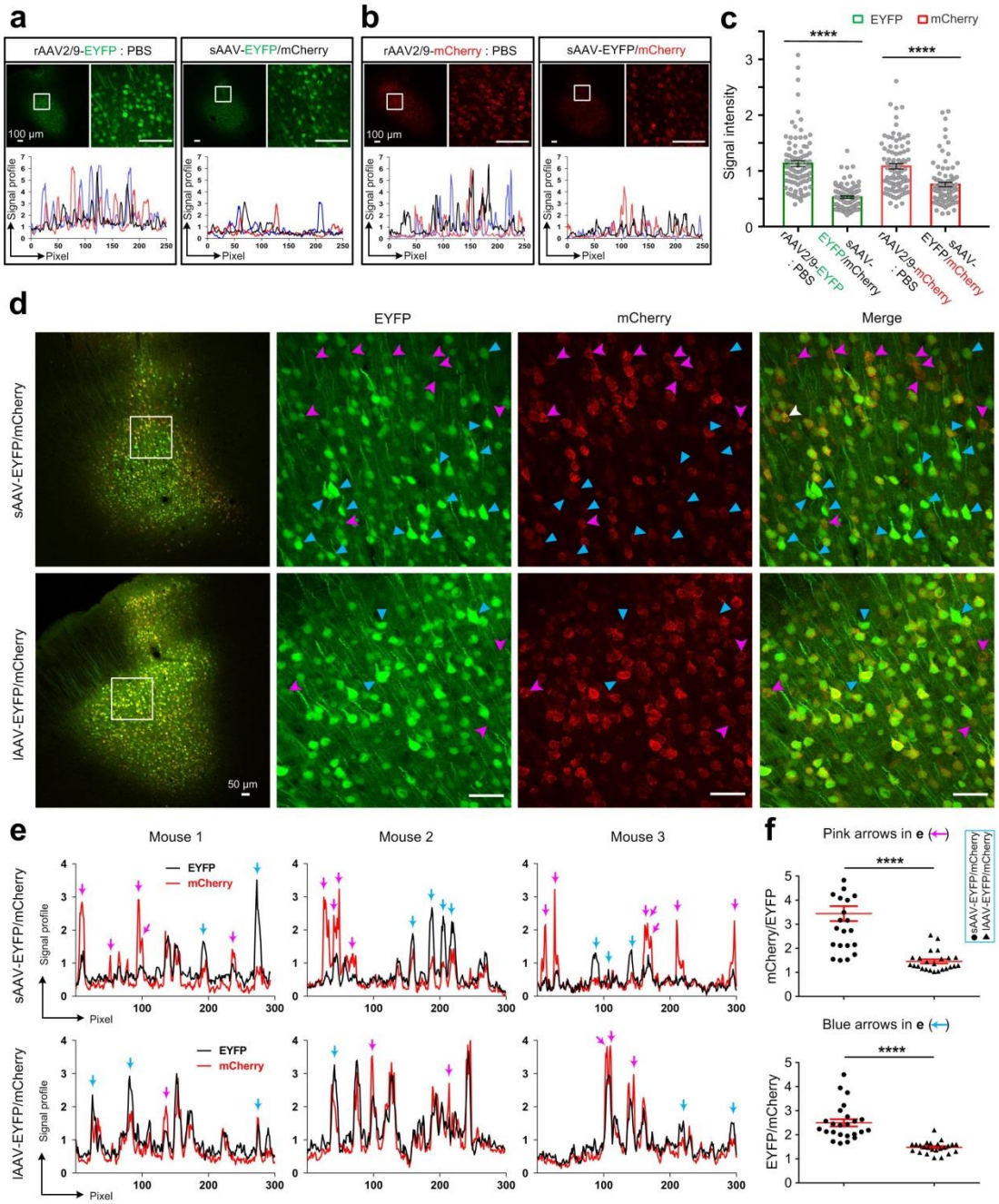

MAP-ENVIVIDERS enables reliable, density-controllable superbright neuronal labeling

Dissection of neurocircuits on individual neuron level is critical for understanding neuronal structure-function relationship and cell-type classification[5]. Dual rAAV-based Cre-lox/Flp-FRT recombinase systems and the tTA/TRE transactivation system have been successfully developed to label limited or tunable numbers of neurons of specific cell types[2-5]. However, a viral copackaging strategy has never been explored in these systems. Therefore, we developed MAP-ENVIVIDERS, a recombinase

system-dependent viral copackaging strategy to enhance the visualization of neurocircuits. We first validated MAP-ENVIVIDERS in wild-type mice with copackaging a Cre-expressing vector and a Cre-dependent vector (**Fig. 2a**). We generated three littermate rAAVs (abbreviated for lAAVs hereafter) by copackaging a CMV promoter-mediated Cre-expressing vector (AAV-CMV-Cre) and a Cre-inducible, double-floxed EYFP element (AAV-double floxed-EYFP)[30] at ratios of 1:20,000 ($lAAV^{20,000}$), 1:200,000 ($lAAV^{200,000}$), and 1:1,000,000 ($lAAV^{1,000,000}$). We found that these three lAAVs produced different labeling densities, but with similar brightness in the soma and long-range axonal projections when injected into the MOp (**Fig. 2b** and **Supplementary Fig. 3**). The labeled somas were well separated, and the fine structures, including various types of spines[31,32] and boutons on local and long-range projecting arborizations[33,34], could be clearly visualized and identified (**Supplementary Fig. 2**).

To compare the differences in labeling efficiency and brightness between lAAVs and mixtures of independently packaged rAAVs (sAAVs), we performed parallel experiments with mixtures of Cre-expressing rAAV and Cre-dependent rAAVs at ratios of 1:20,000, 1:40,000, 1:80,000 and 1:1,000,000 based on previous methods[2] (abbreviated for $sAAV^{20,000}$, $sAAV^{40,000}$, $sAAV^{80,000}$ and $sAAV^{1,000,000}$, see Methods). We selected Thy1-EYFP-H mouse[35], one of widely used transgenic lines as reference. Although density-controllable labeling could be achieved in both lAAVs and sAAVs-based systems, labeling by lAAVs was significantly brighter and more efficient under the same experimental conditions (**Fig. 2c**,**d**). Specifically, the brightness of sparsely labeled neurons by lAAVs (**Supplementary Fig. 1a**,**c**) was equivalent to Thy1-EYFP-H mice, but ~3 times stronger for $lAAV^{200,000}$ compared with $sAAV^{20,000}$ and ~7 times for $lAAV^{1,000,000}$ compared with $sAAV^{1,000,000}$, respectively ($P < 0.001$), demonstrating the sensitivity of MAP-ENVIVIDERS (**Fig. 2d** and **Supplementary Fig. 4**). In accordance with previous study[25], the Cre titers of lAAVs and sAVVs were similar as measured by quantitative polymerase chain reaction, however, the number of labeled neurons for $lAAV^{20,000}$ was nearly 4-fold that of $sAAV^{20,000}$, demonstrating the efficiency of MAP-ENVIVIDERS (**Fig. 2c** and **Supplementary Table 1**). Similar results were also obtained in other brain regions, such as CA1 and CA3, where the labeled neurons were significantly brighter than those in the Thy1-EYFP-H mouse line (**Fig. 2e**, upper and lower right panel; **Supplementary Fig. 5**).

However, the number of neurons labeled differed among the brain regions for the same lAAV preparation (**Fig. 2e**, lower left panel). These results collectively showed that the MAP-ENVIVIDERS labeling strategy is significantly more sensitive, efficient and reproducible than methods using mixtures of independently packaged rAAVs for density-controllable neuron labeling.

To further explore the potential of MAP-ENVIVIDERS in obtaining brain-wide long-range projections, we used fluorescence micro-optical sectioning tomography (TDI-fMOST)[36] to automatically image $lAAV^{200,000}$-labeled MOp whole-brain mouse sample. Imaging was conducted with a voxel size of $0.176 \times 0.176 \times 1\ \mu m^3$, generating 12,841 continuous coronal sections (**Fig. 2f** and **Supplementary Fig. 9**). Among the 11 reconstructed MOp pyramidal neurons, four intratelencephalic neurons located in L2, L3, and L6a projected to the ipsi- and contralateral striatum and cortex, and four pyramidal tract neurons located in L5b projected to diverse subcortical brain regions, as previously reported[37-41] (**Fig. 2h**, **Supplementary Fig. 10a,b** and **Supplementary Video 1**). Interestingly, the remaining three neurons (No. **s1-s3**) formed a novel type of pyramidal neuron located in L5b (**Fig. 2g** and **Supplementary Fig. 10c**). We termed these "boomerang neurons" because they send a collateral axonal branch to the contralateral MOp and dorsal caudoputamen (CP) via the corpus callosum, which then returns to the ipsilateral side via the anterior commissure, innervating the ipsilateral CP region via a collateral on the ipsilateral side, thus forming a symmetrical track (**Fig. 2i**,**j**, **Supplementary Fig. 10d** and **Supplementary Video 2-4**). All of these reconstructed boomerang neurons had complex axonal projections, with over axonal 1,200 branches totaled at ~22 cm long on average (**Supplementary Fig. 11**). Therefore, the use of MAP-ENVIVIDERS together with TDI-fMOST allowed us to document the projectome of individual neurons in great detail as well as to identify novel type of neurons.

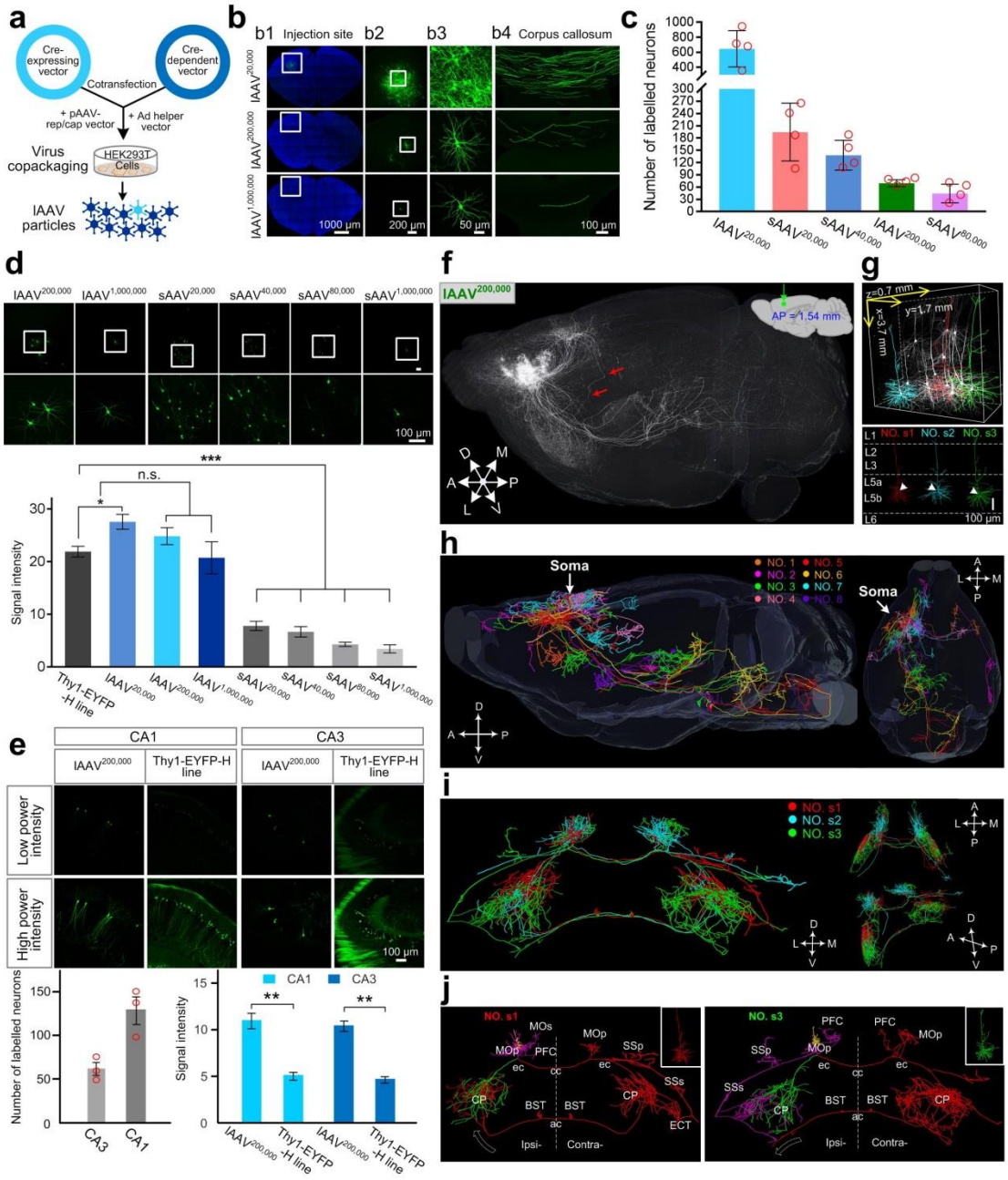

Fig. 2 | MAP-ENVIVIDERS enables density-controllable, superbright neuron labeling and reconstruction of individual MOp neurons in wild-type mice. a, Schematic for the production of lAAVs. Briefly, a Cre-expressing vector and a Cre-expressing vector were mixed at preset ratios on cellular level, generating lAAV particles. **b**, Representative confocal images of neurons from mice injected with 100 nl of lAAVs produced by copackaging pAAV-CMV-Cre and pAAV-EF1α-double floxed-EYFP at the indicated ratios. Images show neurons at the injection sites (**b1-b3**) and their long axonal projections in the corpus callosum (**b4**). **c**, Quantification of neurons labeled by different lAAVs and sAAVs (n = 4 mice each). **d,** Comparison of brightness between neurons labeled by different lAAVs and sAAVs. Upper panel: confocal images; lower panel: quantifications of signal intensities of the labeled somas. Neurons from the Thy1-EYFP-H mouse line were used as a reference (n = 40 cells for the Thy1-EYFP-H mouse line; n = 40 cells for $lAAV^{20,000}$, $lAAV^{200,000}$, $sAAV^{20,000}$, $sAAV^{40,000}$, and

sAAV^{80,000} from 3 mice; n = 20 cells for lAAV^{1,000,000} and n = 17 cells for sAAV^{1,000,000}, from 4 mice). One-way ANOVA with Dunnett's post hoc test. **e**, Applications of lAAV^{200,000} in CA1 and CA3. Comparisons of brightness of lAAV^{200,000}-labeled neurons in CA1 and CA3 (n = 40 cells for each from 3 mice) with Thy1-EYFP-H mouse line (n = 40 cells) were shown with confocal images (upper panel) and measurement of signal intensities (lower right panel) (n = 40 cells for each from 3 mice). Two-tailed t-test. Lower left panel: quantifications of labeled neurons in CA1 and CA3 (n = 3 mice each). **f**, Sagittal view showing lAAV^{200,000}-labeled MOp whole-brain dataset. The red arrows indicate axon pathway of boomerang neurons. **g**, Raw signals (top) and reconstructed dendritic morphologies (bottom) of three boomerang neurons (No. s1-s3). **h**, Summary of axonal morphologies of the eight reconstructed pyramidal neurons (No. 1-8) in sagittal (left panel) and horizontal (right panel) views. **i**, Coronal (left), horizontal (upper right), and sagittal (with a rotated angle, lower right) views showing axonal morphologies of three boomerang neurons. **j**, Localization of the brain-wide axonal projections of neurons **s1** and **s3** (dendrites: yellow; local axons: magenta; the left and right branches originating from the ipsilateral external capsule are shown in green and red, respectively). Dashed white arrows indicate the termination directions of the main axons. All data are presented as the mean ± s.e.m. n.s, non-significant (P > 0.05), *P < 0.05, **P < 0.01, ***P < 0.001. Abbreviations: see **Supplementary Table 2.**

MAP-ENVIVIDERS enables improved neuron labeling in cell-type-specific Cre driver lines

Cell-type-specific labeling is crucial for dissecting the functional role and circuitry of a given type of cell[42]. To demonstrate the potential of MAP-ENVIVIDERS for efficient cell-type-specific and density-controllable labeling with multiple Cre-driver lines, we next redesigned MAP-ENVIVIDERS with an Flp-expressing vector (e.g., AAV-EF1α-Flp) and an Flp- and Cre-dependent vector (e.g., AAV-hSyn Con/Fon EYFP[43]) and copackaged two vectors at different ratios to generate cslAAV^{2,000} and cslAAV^{20,000} (cs refers to cell-type-specific hereafter, **Fig. 3a**). For validations, we injected the resulted two cslAAVs into MOp of Thy1-Cre transgenic mice and found that tunable neuron labeling was achieved with different ratios (**Supplementary Fig. 6a**,**b**), indicating the functionality of MAP-ENVIVIDERS with Cre-driver transgenic lines.

To achieve cell-type-specific sparse and superbright labeling of cholinergic neurons, we next applied one of cslAAVs, cslAAV^{20,000} into the basal forebrain (BF) of choline acetyltransferase (ChAT)-Cre transgenic mice[44] (**Fig. 3b**). Among 54 ± 4 well-separated neurons labeled with cslAAV^{20,000} (n = 4 mice), 97.6 ± 1.6% of which were

ChAT positive (**Fig. 3c**, **Supplementary Fig. 7** and **Supplementary Table 1**). Fine structures of these sparsely neurons, both near and far from the somas, could be visualized clearly (**Fig. 3d-h**) and their fine long-range projections covered diverse brain regions as previously reported[45] (**Supplementary Fig. 8**). Parallel experiments with wild-type mice did not label any cells (n = 4 mice; **Supplementary Fig. 6c**), confirming the cell-type specificity of the method. In another set of parallel experiments in which $cssAAV^{2,000}$ and $cssAAV^{20,000}$, mixtures of the corresponding independently packaged rAAVs (see Methods) were injected into BF of ChAT-Cre transgenic mice. We found that no neurons were labeled with $cssAAV^{20,000}$ and only a few faintly labeled with $cssAAV^{2,000}$ (n = 5 mice each; **Supplementary Fig. 6d**,**e**). These results demonstrated that the MAP-ENVIVIDERS strategy was significantly more sensitive and efficient for cell-type-specific neuron labeling.

We also performed whole-brain mapping of BF-injected brains of ChAT-Cre mice. The sparse but super-bright labeling enabled us to visualize the detailed morphology of each neuron (**Fig. 3i**). All three reconstructed cholinergic neurons showed rather complex projectomes, with an average of 4,531 axonal branches totaled ~30 cm long (**Fig. 3j**, **Supplementary Fig. 11** and **Supplementary Video 5**). In particular, No. **c2** had a total length of 49.1 cm and exhibited massive arborizations in the lateral visual area (VISl) and subiculum (SUB), with ~7,840 and 1,660 axonal branches, respectively (**Fig. 3k** and **Supplementary Video 6**). These results demonstrate that the MAP-ENVIVIDERS could capture morphological details of individual neurons with cell-type specificity to a great extent.

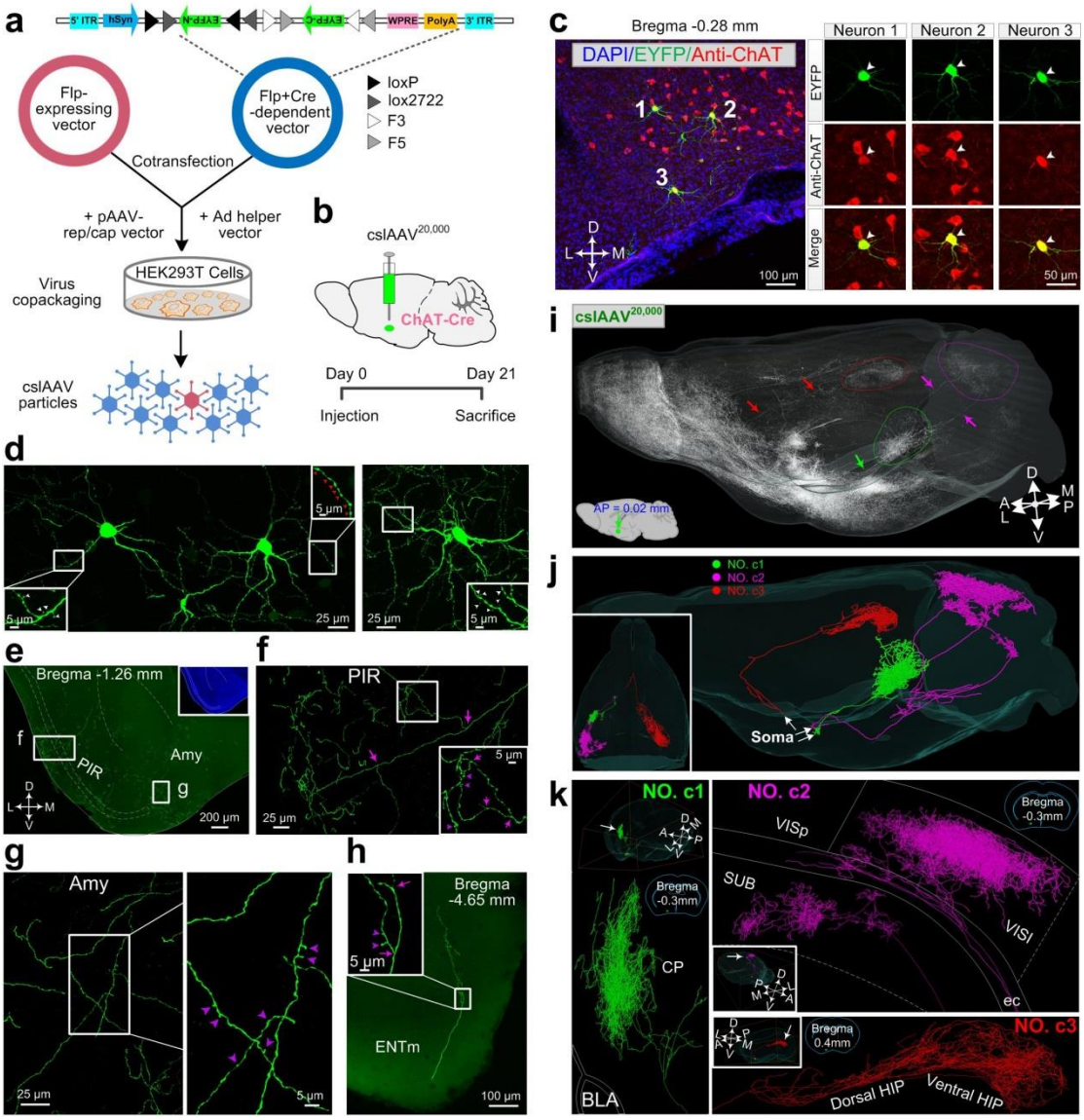

Fig. 3 | MAP-ENVIVIDERS enables cell-type-specific sparse but superbright labeling in transgenic mice, allowing reconstruction of individual neurons. **a**, Schematic showing the generation of cslAAVs and the Cre- and Flp-dependent AAV vector. ITR, inverted terminal repeat; hSyn, human synapsin promoter; WPRE, woodchuck hepatitis virus post transcriptional regulatory element. **b**, Schematic of the experiment for the data in **c**-**k**. **c**, Low-magnification (left) and high-magnification (right) images showing colocalization of three cholinergic neurons (labeled neurons 1 to 3, green) with anti-ChAT antibody staining (red). **d**, Fine structure of three cholinergic neurons. Insets are enlargements of the corresponding boxes, white arrowheads indicate spines, and red arrowheads indicate boutons. **e**-**h**, Representative images showing long-range axonal projections in the piriform cortex (PIR, **f**), amygdala (Amy, **g**), and medial entorhinal cortex (ENTm, **h**). **i**, Sagittal view showing whole-brain labeling after injection of cslAAV^{20,000} into the basal forebrain. Arrows indicate the main axons, and colored circles indicate the terminal arborizations of each reconstructed neuron. **j**, Summary of the axonal morphologies of three reconstructed cholinergic neurons (No. c1-c3) in sagittal and the

horizontal view (insets). **k**, High-magnification images of complex axonal arborizations (indicated by white arrows) of neurons c1-c3. Abbreviations: see Supplementary Table 2.

MAP-ENVIVIDERS substantially improves the efficiency of RV-mediated monosynaptic tracing systems

The current RV-mediated trans-monosynaptic tracing systems involve two different processes: the entry of EnvA-pseudotyped, rabies glycoprotein (RG)-deleted RV (EnvA-RVΔG) into the cells through the interaction of EnvA with TVA delivered by one rAAV, and the assembly of infectious RV particles by providing RVΔG with the RG delivered by another rAAV[6-9]. Based on the earlier results (**Figs. 1-3**), the enhanced compatibility conferred by AAV copackaging should improve the coherence between the TVA-EnvA interaction and RVΔG-RG assembly, leading to a significant increase in the efficiency of trans-monosynaptic labeling with the prevalent rAAV-RV combination system. To test this hypothesis, we redesigned MAP-ENVIVIDERS with two Cre-dependent vectors, AAV-DIO-EGFP-TVA (GT) and AAV-DIO-RG (**Fig. 4a**). As an example, we copackaged AAV-DIO-GT and AAV-DIO-RG at a ratio of 1:2 to generate littermate virus, termed lAAV-DIO-GT/RG. The labeling efficiency was compared with that obtained using the two vectors packaged independently and mixed at a ratio of 1:2 (sAAV-DIO-GT/RG, **Fig. 4b**).

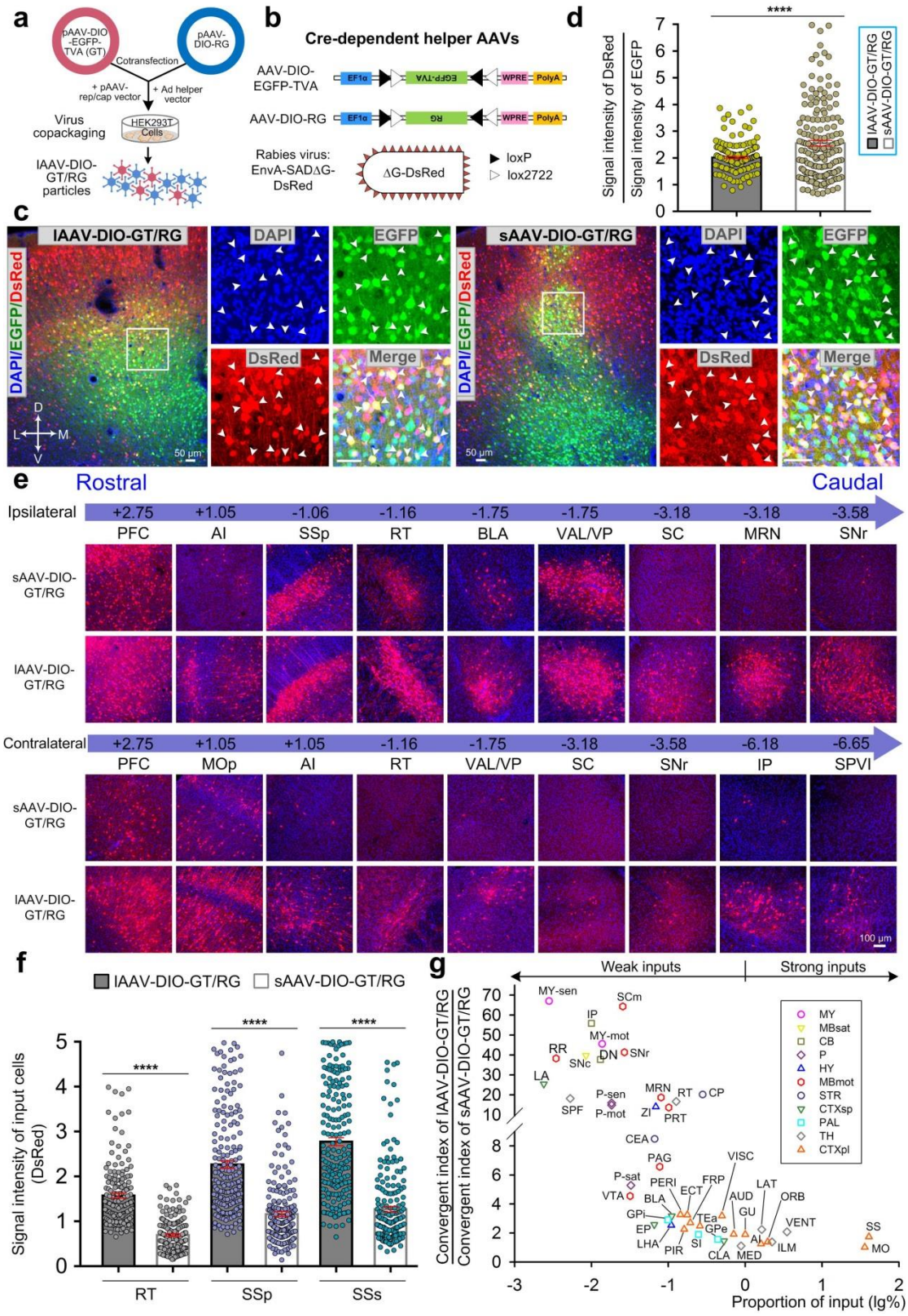

Fig. 4 | MAP-ENVIVDERS enables efficient tracing of input networks. a, Schematic for generating lAAV-DIO-GT/RG, two Cre-dependent AAV vectors for the respective expression of TVA and RG were premixed at a ratio of 1:2. **b**, Schematic of the two Cre-dependent rAAV helpers and the EnvA-pseudotyped rabies virus. **c**, Representative coronal sections showing the injection site in lAAV-DIO-

GT/RG- and sAAV-DIO-GT/RG-labeled mice. Boxed regions show colocalization of DAPI (blue), EGFP (green), and DsRed (red). White arrowheads indicate triple-positive neurons. **d**, Comparison of the ratio between the signal intensity of DsRed and EGFP in starter cells labeled by lAAV-DIO-GT/RG and sAAV-DIO-GT/RG, n = 170 neurons from 3 mice for both groups. **e**, Representative images showing ipsi- and contralateral input neurons in different brain regions labeled by RV via lAAV-DIO-GT/RG or sAAV-DIO-GT/RG. **f**, Signal intensities of input neurons in RT, SSp, and SSs labeled by lAAV-DIO-GT/RG-RV or sAAV-DIO-GT/RG-RV. n = 160 neurons for RT, n = 190 neurons for SSp and SSs, n =3 mice for both groups. **g**, Relationship between the proportion of inputs (input cells in each subregion relative to the total input cells across whole brain, which was denoted by logarithm to base 10 (lg %, x-axis) and the enhanced ratios provided by MAP-ENVIVIDERS (the ratio between convergent index of lAAV-DIO-GT/RG and convergent index of sAAV-DIO-GT/RG, y-axis). Data are presented as mean ± s.e.m.; two-tailed t-test ****P < 0.0001. Abbreviations: see Supplementary Table 2.

Equal volume of lAAV-DIO-GT/RG or sAAV-DIO-GT/RG was injected into the MOp of Thy1-Cre transgenic mice, followed by the injection of EnvA-pseudotyped RV 21 days later. Nine days after the second injection, the mice were sacrificed for analysis. The numbers of $EGFP^+/DsRed^+$ starter cells in lAAV-DIO-GT/RG and sAAV-DIO-GT/RG groups were similar (2,386 ± 172 vs. 2,039 ± 127, n = 5 animals each; **Fig. 4c** and **Supplementary Table 3**) and the value of the DsRed/EGFP ratio closely matched the preset ratio of 2:1 for the lAAV-DIO-GT/RG group but significantly deviated from 2:1 for the sAAV-DIO-GT/RG group (**Fig. 4d** and **Supplementary Fig. 1b**,**c**; 2.01 ± 0.04 versus 2.67 ± 0.13; mean ± s.e.m., unpaired t-test, P < 0.0001, n = 3 mice) on the group level. Furthermore, the distribution of ratios in individual neurons was significantly narrower for lAAV-DIO-GT/RG than sAAV-DIO-GT/RG (**Fig. 4d**). For trans-synaptic labeling, efficiency was generally increased across the entire brain. The improvement granted by the MAP-ENVIVIDERS system was most prominent for highly underrepresented regions far from the injection site, such as the reticular nucleus of the thalamus (RT), the superior colliculus (SC), the midbrain reticular nucleus (MRN), and the substantia nigra pars reticulata (SNr) on the ipsilateral side and all regions on the contralateral side, especially the interposed nucleus (IP) and the spinal nucleus of the trigeminal nerve, subnucleus interpolaris (SPVI) (**Fig. 4e** and **Supplementary Fig. 12**,**13**). MAP-ENVIVIDERS also improved the labeling moderately in the brain regions that were well-labeled by the classical sAAV-DIO-GT/RG-RV combination, such as the prefrontal cortex (PFC), the primary somatosensory area (SSp), and the ventral anterior-lateral complex of the thalamus (VAL)/ventral posterior complex of the thalamus (VP).

To compare the global tracing efficiency of the two systems quantitatively, the whole brain (Bregma +3.25 to -7.25) was divided into 11 major regions containing 44 subregions according to the Allen Mouse Brain Atlas[46,47]. We registered the numbers of labeled DsRed+ input cells and calculated the corresponding convergent index[18] (the number of input cells divided by the number of starter cells) in each subregion. Subsequently, we plotted the ratio between convergent index of lAAV-DIO-GT/RG and convergent index of sAAV-DIO-GT/RG against the percentage of inputs (input cells in each region relative to the total input cells across whole brain) within sAAV-DIO-GT/RG labeled groups. We found that the relationship between the improvement and the labeling efficiency by MAP-ENVIVIDERS is clear: the poorer the labeling with the original sAAV-DIO-GT/RG-RV combination system, the greater the improvement could be achieved by MAP-ENVIVIDERS (**Fig. 4g** and **Supplementary Fig. 14a-d**). Generally, most of the regions that were underrepresented originally (< 1%) were enhanced by more than an order of magnitude. These regions with dramatic (> 10-fold) improvements were distributed throughout 40% of all input subregions, which were more frequently found in midbrain, pons, medulla and cerebellum (**Supplementary Fig. 14e**). Remarkably, the brain stem showed particular improvements of up to 70-fold (**Fig. 4g** and **Supplementary Fig. 14d**). We further measured the signal intensities of the input neurons in several brain regions, including RT, SSp and supplemental somatosensory area (SSs) within two labeling groups (**Supplementary Fig. 1d**). We found that DsRed signals of input neurons were significantly enhanced (averaged 2-fold) within lAAV-DIO-GT/RG groups when compared with sAAV-DIO-GT/RG groups (**Fig. 4f**; 2.27-fold for RT, 1.94-fold for SSp and 2.19-fold for SSs; unpaired t-test, $P < 0.0001$, $n = 3$ mice). These data collectively showed that MAP-ENVIVIDERS significantly enhanced not only the number but also the brightness of the labeled input neurons. Taken the facts of similar number of starter cells, significantly enhanced number and fluorescent intensity of input cells suggest that many more RVs are produced by the starter cells in MAP-INVIVIDERS.

DISCUSSION

In the present study, we found that strong mutual suppression existed among independently packaged rAAVs and copackaging of rAAV-producing plasmids enhanced co-expression of genes among multiple AAVs. We then developed the MAP-ENVIVIDERS providing improved superbright and sparse labeling for certain types of neurons and more efficient cell-type-specific whole-brain input mapping.

MAP-ENVIVIDERS were more prominent in complicated systems requiring co-expression of multiple rAAVs. For non-cell-type-specific superbright and sparse labeling (co-expression of Cre and Cre-dependent fluorescent protein), MAP-ENVIVIDERS provided ~3-fold more labeled neurons and ~5-fold more bright fluorescent intensity. For cell-type-specific superbright and sparse labeling (co-expression of Flp, Cre and Flp-/Cre-dependent fluorescent protein), MAP-ENVIVIDERS was estimated to provide more than 10-fold increase of labeling efficiency. Thus, MAP-ENVIVIDERS could achieve the same efficiency with much lower dose of virus, which may reduce cytotoxicity and experimental cost. Notably, since MAP-ENVIVIDERS is very sensitive, careful consideration of mixing ratios for viral copackaging was needed to label desired number of neurons. For cell-type-specific superbright/sparse labeling, the strength and abundance of Cre recombinase varies greatly among different cell types and brain regions[44], thus the mixing ratio of Flp and Flp-/Cre-dependent fluorescent protein need to be carefully tested.

MAP-ENVIVIDERS also provided a dramatical increase (10- to 70-fold) of cell-type-specific whole-brain input mapping for 40% of the input brain regions (sparsely labeled by previous strategies). The much stronger DsRed signals and the larger number of total input neurons suggested that more RVs may be produced with the MAP-ENVIVIDERS strategy. This is probably due to the reduction of mutual suppression between the rAAVs expressing TVA and RG. The AAVs in the starter cells expressed more TVA and RG, leading to more entry and assemble of infectious RVs and eventually higher transsynaptic tracing efficiency (convergent index from averaged 32 to 52, **Supplementary Table 3**). Moreover, it is feasible to combine MAP-ENVIVIDERS with optimized RG (oG)[48] and other RV strains (e.g., the CVS-N2c$^{\Delta G}$ strain)[10] to further improve the tracing efficiency.

Though further efforts are needed to explore the underlying mechanisms, the probable reasons leading to the high sensitivity and efficiency of MAP-ENVIVIDERS were

speculated as follows: (i) Viral copackaging strategy will reduce the heterogeneity of impurities, including cyto-toxins, cellular fragments and proteins, and culture media residues deprived from viral preparations of independently packaged rAAVs, thus reduce effect of strong immune responses on the state of the host cells near the injection site[21-23]. (ii) Gene cassettes delivered by cocktails of rAAVs with different serotypes may elicit different immune responses, leading to varying reductions in gene expression[49,50], which could be avoided by viral copackaging. (iii) The amplification of signals by recombinase systems combined with effects of (i) and (ii) reasonably leads to significant improvements of efficiency.

Besides the anatomical studies, MAP-ENVIVIDERS is suitable for functional studies of neural circuitry[12,13] and may even be used in other organs beyond mammal brain. Furthermore, MAP-ENVIVIDERS also provides great potential to facilitate the co-expression of multiple genes and reduce the harmful effects for clinical gene therapy[51-56].

Acknowledgements

We thank Qing Liu, Huadong Wang, Zhijian Zhang and Fan Jia from Wuhan Institute of Physics and Mathematics, CAS Center for Excellence in Brain Science and Intelligence Technology, Chinese Academy of Sciences for comments on the manuscript. We thank Prof. Hui Gong, Yandong Gang, Feng Xiong, Ru Guo, Fei Huang, Siqi Jiang, Xue Peng and Wu Chen from the Wuhan National Laboratory for Optoelectronics, Huazhong University of Science and Technology for help with whole-brain imaging and data analysis. We also thank the Optical Bioimaging Core Facility of WNLO-HUST and the Analytical and Testing Centre of HUST for the support in data acquisition. This work was supported by the National Basic Research Program of China (Grants No. 2015CB755601), the National Natural Science Foundation of China (Grant No. 31470056, 31830035, 31871051), the Science Fund for Creative Research Group of China (Grant No. 61721092), the Strategic Priority Research Program (B), Chinese Academy of Sciences (Grants No. XDB32030200), Science and Technology Planning Project of Guangdong Province (Grants No. 2018B030331001), and the Director Fund of the Wuhan National Laboratory for Optoelectronics.

Authors' Contributions

F.X. and Y.-H.Z conceived of the project. P.S., S.J., S.T. and J.P. performed

experiments. P.S., S.J. and J.W. analysed the data. F.X., P.S. and S.J. designed all the viruses. X.H., Z.L. and Y.W. contributed to the production of the viruses. Y.L. conducted the resin embedding. N.L., X.L. and X.L. performed the whole-brain imaging. P.S., H.L. and J.K. contributed to neuronal reconstructions. L.W., M.X. and S.Z. afford technical assistance with whole-brain tracing of input neurons. S.Z., X.L. and A.L. supervised the image preprocessing and data analysis of whole-brain data. Y.-H.Z., F.X. and P.S. wrote the manuscript with discussion and improvements from all authors.

Competing financial interests.

The authors declare no competing financial interests.

RENFERENCES

1. Samulski, R. J. & Muzyczka, N. AAV-Mediated Gene Therapy for Research and Therapeutic Purposes. *Annu. Rev. Virol.* **1**, 427–451 (2014).

2. Economo, M. N. *et al*. A platform for brain-wide imaging and reconstruction of individual neurons. *eLife* **5**, e10566 (2016).

3. Lin, R. *et al*. Cell-type-specific and projection-specific brain-wide reconstruction of single neurons. *Nat. Methods* **15**, 1033–1036 (2018).

4. Sakaguchi, R., Leiwe, M. N. & Imai, T. Bright multicolor labeling of neuronal circuits with fluorescent proteins and chemical tags. *eLife* **7**, 40350 (2018).

5. Luo, L., Callaway, E. M. & Svoboda, K. Genetic dissection of neural circuits: a decade of progress. *Neuron* **98**, 256–281 (2018).

6. Schwarz, L. A. *et al*. Viral-genetic tracing of the input-output organization of a central noradrenaline circuit. *Nature* **524**, 88–92 (2015).

7. Watabe-Uchida, M., Zhu, L., Ogawa, S. K., Vamanrao, A. & Uchida, N. Whole-brain mapping of direct inputs to midbrain dopamine neurons. *Neuron* **74**, 858–873 (2012).

8. Miyamichi, K. *et al.* Dissecting local circuits: parvalbumin interneurons underlie broad feedback control of olfactory bulb output. *Neuron* **80**, 1232–1245 (2013).

9. Weissbourd, B. *et al.* Presynaptic partners of dorsal raphe serotonergic and GABAergic neurons. *Neuron* **83**, 645–662 (2014).

10. Reardon, T. R. *et al.* Rabies virus CVS-N2c strain enhances retrograde synaptic transfer and neuronal viability. *Neuron* **89**, 711–724 (2016).

11. Tovote, P. *et al*. Midbrain circuits for defensive behaviour. *Nature* **534**, 206–212 (2016).

12. Wang, W. *et al*. A light- and calcium-gated transcription factor for imaging and manipulating activated neurons. *Nat. Biotechnol.* **35**, 864–871 (2017).

13. Lee, D., Hyun, J. H., Jung, K., Hannan, P. & Kwon, H. B. A calcium and light-gated switch to induce gene expression in activated neurons. *Nat. Biotechnol. 35*, 858–863 (2017).

14. Bedbrook, C. N., Deverman, B. E. & Gradinaru, V. Viral strategies for targeting the central and peripheral nervous systems. *Annu. Rev. Neurosci.* **41**, 323–348 (2018).

15. Kotterman, M. A. & Schaffer, D. V. Engineering adeno-associated viruses for clinical gene therapy. *Nat. Rev. Genet.* **15**, 445–451 (2014).

16. Sun, S. & Schaffer, D. V. Engineered viral vectors for functional interrogation, deconvolution, and manipulation of neural circuits. *Curr Opin Neurobiol.***50**, 163-170 (2018).

17. Callaway, E. M. & Luo, L. Monosynaptic circuit tracing with glycoprotein-deleted rabies viruses. *J. Neurosci.* **35**, 8979–8985 (2015).

18. Miyamichi, K. *et al.* Cortical representations of olfactory input by trans-synaptic tracing. *Nature* **472**, 191–196 (2011).

19. Zolotukhin, S. *et al.* Recombinant adeno-associated virus purification using novel methods improves infectious titer and yield. *Gene Ther.* **6**, 973–985(1999).

20. Ayuso, E. *et al.* High AAV vector purity results in serotype- and tissue-independent enhancement of transduction efficiency. *Gene Ther.* **17**, 503–510 (2010).

21. Schnodt, M. & Buning, H. Improving the quality of adeno-associated viral vector preparations: the challenge of product-related impurities. *Hum. Gene Ther. Methods* **28**, 101–108 (2017).

22. Bantel-Schaal, U. & H, zur Hausen. Adeno-associated viruses inhibit SV40 DNA amplification and herpes simplex virus replication in SV40-transformed hamster cells. *Virology* **164**, 64–74 (1988).

23. Timpe, J. M., Verrill, K. C. & Trempe, J. P. Effects of adeno-associated virus on adenovirus replication and gene expression during coinfection. *J. Virol.* **80**, 7807-7815 (2006).

24. Criddle, A., Thornburg, T., Kochetkova, I., DePartee, M. & Taylor, M. P. gD-independent superinfection exclusion of alphaherpesviruses. *J. Virol.* **90**, 4049–4058 (2016).

25. Kim, J. S., Enquist, L. W. & Card, J. P. Circuit-specific coinfection of neurons in the rat central nervous system with two pseudorabies virus recombinants. *J. Virol.* **73**, 9521–9531 (1999).

26. Kobiler, O., Lipman, Y., Therkelsen, K., Daubechies, I. & Enquist, L.W. Herpesviruses carrying a Brainbow cassette reveal replication and expression of limited numbers of incoming genomes. *Nat. Commun.* **1**, 146 (2010).

27. Pan, C. *et al.* Shrinkage-mediated imaging of entire organs and organisms using uDISCO. *Nat. Methods* **13**, 859-867 (2016).

28. Doerfler, P. A., Byrne, B. J. & Cle ́ment, N. Copackaging of Multiple Adeno-Associated Viral Vectors in a Single Production Step. *Hum. Gene Ther. Methods* **25**, 269–276 (2014).

29. Wang, Q. *et al.* Efficient production of dual recombinant adeno-associated viral vectors for factor VIII delivery. *Hum Gene Ther Methods* **25**, 261–268 (2014).

30. Sohal, V. S., Zhang, F., Yizhar, O. & Deisseroth, K. Parvalbumin neurons and gamma rhythms enhance cortical circuit performance. *Nature* **459**, 698–702 (2009).

31. Spruston, N. Pyramidal neurons: dendritic structure and synaptic integration. *Nat. Rev. Neurosci.* **9**, 206–221 (2008).

32. Holtmaat, A. & Svoboda, K. Experience-dependent structural synaptic plasticity in the mammalian brain. *Nat. Rev. Neurosci.* **10**, 647–658 (2009).

33. Stettler, D. D., Yamahachi, H., Li, W., Denk, W. & Gilbert, C. D. Axons and synaptic boutons

are highly dynamic in adult visual cortex. *Neuron* **49**, 877–887 (2006).

34. De Paola, V. *et al.* Cell type-specific structural plasticity of axonal branches and boutons in the adult neocortex. *Neuron* **49**, 861–875 (2006).

35. Feng, G. *et al.* Imaging neuronal subsets in transgenic mice expressing multiple spectral variants of GFP. *Neuron* **28**, 41–51 (2000).

36. Xiong, H. *et al.* Whole mouse brain fluorescence imaging at synaptic resolution (in preparations).

37. Mao, T. *et al.* Long-range neuronal circuits underlying the interaction between sensory and motor cortex. *Neuron* **72**, 111–123 (2011).

38. Kita, T. & Kita, H. The subthalamic nucleus is one of multiple innervation sites for long-range corticofugal axons: a single-axon tracing study in the rat. *J. Neurosci.* **32**, 5990–5999 (2012).

39. Jeong, M. *et al.* Comparative three-dimensional connectome map of motor cortical projections in the mouse brain. *Sci. Rep.* **6**, 20072 (2016).

40. Shepherd, G. M. Corticostriatal connectivity and its role in disease. *Nat. Rev. Neurosci.* **14**, 278–291 (2013).

41. Harris, K. D. & Shepherd, G. M. The neocortical circuit: themes and variations. *Nat. Neurosci.* **18**, 170–181 (2015).

42. Huang, Z. J. & Zeng, H. Genetic approaches to neural circuits in the mouse. *Annu. Rev. Neurosci.* **36**, 183–215 (2013).

43. Fenno, L. E., Mattis, J., Ramakrishnan, C. & Deisseroth, K. (2017). A guide to creating and testing new INTRSECT constructs. *Curr. Protoc. Neurosci.* **80**, 4.39.1–4.39.24 (2017).

44. Gong, S. *et al.* Targeting Cre recombinase to specific neuron populations with bacterial artificial chromosome constructs. *J. Neurosci.* **27**, 9817–9823 (2007).

45. Li, X. *et al.* Generation of a whole-brain atlas for the cholinergic system and mesoscopic projectome analysis of basal forebrain cholinergic neurons. *Proc. Natl Acad. Sci. USA* **115**, 415–420 (2018).

46. Zhang, S. *et al.* Organization of long-range inputs and outputs of frontal cortex for top-down control. *Nat. Neurosci.* **19**, 1733–1742 (2016).

47. Do, J. P. *et al.* Cell type-specific long-range connections of basal forebrain circuit. *eLife* **5**, e13214 (2016).

48. Kim, E. J., Jacobs, M. W., Ito-Cole, T. & Callaway, E. M. Improved monosynaptic neural circuit tracing using engineered rabies virus glycoproteins. *Cell Rep.***15**, 692-699 (2016).

49. Kotterman, M. A., Chalberg, T. W. & Schaffer, D. V. Viral vectors for gene therapy: translational and clinical outlook. *Annu. Rev. Biomed. Eng.* **17**, 63–89 (2015).

50. Naso, M. F., Tomkowicz, B., Perry, W. L., III, & Strohl, W. R. Adeno-associated virus (AAV) as a vector for gene therapy. *BioDrugs* **31**, 317-334 (2017).

51. Kotterman, M. A. & Schaffer, D. V. Engineering adeno-associated viruses for clinical gene therapy. *Nat. Rev. Genet.* **15**, 445–451 (2014).

52. Yang, Y. *et al.* A dual AAV system enables the Cas9-mediated correction of a metabolic liver disease in newborn mice. *Nat. Biotechnol.* **34**, 334–338 (2016).
53. Lai, Y. *et al.* Efficient in vivo gene expression by trans-splicing adeno-associated viral vectors. *Nat. Biotechnol.* **23**, 1435–1439 (2005).
54. Maddalena, A. *et al.* Triple Vectors Expand AAV Transfer Capacity in the Retina. *Mol. Ther.* **26**, 524-541 (2018).
55. McClements, M. E. & MacLaren, R. E. Adeno-associated virus (AAV) dual vector strategies for gene therapy encoding large transgenes. *Yale J. Biol. Med.* **90**, 611–623 (2017).
56. Grieger, J. C., Choi, V. W. & Samulski, R. J. Production and characterization of adeno-associated viral vectors. *Nat. Protoc.* **1**, 1412–1428 (2006).
57. Osakada, F. & Callaway, E. M. Design and generation of recombinant rabies virus vectors. *Nat. Protoc.* **8**, 1583–1601 (2013).
58. Paxinos, G. & Franklin, K. B. J. The Mouse Brain in Stereotaxic Coordinates (Academic Press, 2001).
59. Xiong, H. *et al.* Chemical reactivation of quenched fluorescent protein molecules enables resin-embedded fluorescence microimaging. *Nat. Commun.* **5**, 3992 (2014).
60. Gong, H. *et al.* High-throughput dual-colour precision imaging for brain-wide connectome with cytoarchitectonic landmarks at the cellular level. *Nat. Commun.* **7**, 12142 (2016).

METHODS

Animals. All animal experimental procedures were approved by the Institutional Animal Ethics Committee of Huazhong University of Science and Technology (HUST) and Wuhan Institute of Physics and Mathematics (WIPM). All mice used in this study were 2-month-old male mice, including C57BL/6J mice, Thy1-EYFP-H line transgenic mice (Jackson Laboratory, stock number 003782, USA), Thy1-Cre transgenic mice (Jackson Laboratory, stock number 006143, USA) and ChAT-Cre transgenic mice (Jackson Laboratory, stock number 006410, USA).

Virus preparations. All viruses used in this study were customized or commercially provided by BrainVTA Science and Technology Company (Wuhan, China). Three general types of viruses were used: copackaged littermate AAVs (lAAVs, l refers to littermate) for enhancing viral compatibility and coherence among different viruses, independently packaged stranger AAVs (sAAVs, s refers to stranger) as control, and genetically modified RV (EnvA-SADΔG-DsRed) for retrograde trans-monosynaptic labeling. Production of rAAVs and genetically modified RV were prepared as previously described[56,57].

Both general types of AAVs were serotype 2/9. They were used for four purposes: (i) verification of viral interactions, enhancing infection and exogenous gene expression efficiency for (ii) non-cell-type-specific and (iii) cell-type-specific neuronal labeling, as well as for (iv) trans-monosynaptic labeling of the direct input network of specific type of starter cells. For purpose (i), plasmids AAV-EF1α-EYFP and AAV-EF1α-mCherry were copackaged at a 1:1 ratio or independently packaged in HEK293T cells, generating the corresponding littermate rAAV2/9-EF1α-EYFP/mCherry (abbreviated for lAAV-EFYP/mCherry for convenience). As controls, the two stranger rAAVs, rAAV2/9-EF1α-EYFP and rAAV2/9-EF1α-mCherry, were mixed at a 1:1 ratio before experiments (abbreviated for sAAV-EFYP/mCherry). Parallel experimental procedures were carried out for purposes (ii) to (iv), but with different plasmids at different ratios. For purpose (ii), the plasmids were AAV-EF1α-double floxed-EYFP-WPRE-HGHpA[30] (Addgene #20296, a generous gift from Dr. Karl Deisseroth, Stanford University) and AAV-CMV-Cre. The littermate rAAVs were $lAAV^{20,000}$, $lAAV^{200,000}$ and $lAAV^{1,000,000}$. As controls, one of the two stranger rAAVs, rAAV2/9-CMV-Cre, was initially diluted to ratios of 1:20,000, 1:40,000, 1:80,000 and 1:1,000,000 in phosphate-buffered saline (PBS) before mixed equally with the other stranger rAAV, rAAV2/9-EF1α-double floxed-EYFP (the resulting

rAAVs were abbreviated for sAAV^{20,000}, sAAV^{40,000}, sAAV^{80,000} and sAAV^{1,000,000}, respectively). For purpose (iii), the plasmids were AAV-hSyn Con/Fon EYFP[43] (Addgene #55650, a generous gift from Dr. Karl Deisseroth, Stanford University) and AAV-EF1α-Flp. The littermate rAAVs were cslAAV^{2,000} and cslAAV^{20,000} (cs refers cell-type-specific). Similarly, one of the two stranger rAAVs, rAAV2/9-EF1α-Flp, was diluted to ratios of 1:2,000 and 1:20,000 in PBS, followed by equal mixing with the other stranger rAAV, rAAV2/9-hSyn Con/Fon EYFP (the resulting rAAVs were abbreviated for cssAAV^{2,000} and cssAAV^{20,000}, respectively). For purpose (iv), the plasmids were AAV-EF1α-DIO-EGFP-TVA (GT) and AAV-EF1α-DIO-RG, and the littermate rAAVs, lAAV-DIO-GT/RG, had a ratio of 1:2. For the preparation of stranger rAAVs (sAAV-DIO-GT/RG), rAAV2/9-EF1α-DIO-GT and rAAV2/9-EF1α-DIO-RG were mixed at a ratio of 1:2. The concentrations of the plasmids and the titers of all viruses are listed in Supplementary Table 4.

Virus injections. All virus injection experiments were performed in Biosafety level 2 (BSL-2) environments. Mice were placed into a stereotaxic apparatus (#68030, RWD Life Science, China) and fixed with a nose clamp and ear bars after being deeply anesthetized by isoflurane. A small hole was made over the skull via a dental drill following the incision of the scalp along the midline of the brain. The coordinates for the injections were as follows based on *The Mouse Brain in Stereotaxic Coordinates*[58]: MOp (AP: 1.54 mm; ML: -1.6 mm; DV: -1.6 mm); CA3 (AP: -1.7 mm; ML: -2.0 mm; DV: -2.0 mm); CA1 (AP: -1.7 mm; ML: -1.0 mm; DV: -1.5 mm); and basal forebrain: (AP: 0.21 mm; ML: -1.5 mm; DV: -5.5 mm).

For comparisons of sAAV-EFYP/mCherry with pure rAAVs (**Fig. 1a-c**) and sAAV-EFYP/mCherry with lAAV-EFYP/mCherry (**Fig. 1d-f**), similar titers of sAAV-EFYP/mCherry, rAAV2/9-EF1α-EYFP/PBS mixture (ratio of 1:1) and rAAV2/9-EF1α-mCherry/PBS mixture with a volume of 100 nl were injected into the MOp of C57BL/6J mice. For non-cell-type-specific and cell-type-specific neuronal labeling, 100 nl littermate rAAVs (lAAVs and cslAAVs) and stranger rAAVs (sAAVs and cssAAVs) were injected for C57BL/6J mice (**Fig. 2** and **Supplementary Figs. 2-5**,**6c**,**9-11**) and Cre-driver transgenic lines (**Fig. 3** and **Supplementary Figs. 6a**,**b**,**d**,**e**,**7**,**8**,**11**). For comparisons of transsynaptic spreading efficiency (**Fig. 4** and **Supplementary Figs. 12-14**), the procedures for MAP-ENVIVIDERS and the classical rAAV-RV systems were similar to the reported[46,47], with injected volume as 80 nl for both lAAV-DIO-GT/RG and sAAV-DIO-GT/RG. Three weeks later, 150 nl

EnvA-SADΔG-DsRed was injected into the same site of Thy1-Cre transgenic mice.

All virus solutions used were injected with a pulled glass micropipette at a rate of 20 nl/ min. The micropipette remained in place for at least 5 min before withdrawal from the brain. After recovery, the mice were housed carefully until perfusion.

Perfusion and slicing. Three weeks after AAV injections and nine days after rabies virus injections, mice were perfused transcardially with 0.01 M PBS followed by 4% paraformaldehyde (PFA) in 0.01 M PBS. The extracted intact brains were postfixed overnight at 4°C and placed in 30% sucrose for 48-72 h, and 50-μm frozen sections were maintained across the whole brain (except that one mouse of $lAAV^{1,000,000}$ where sections of injection site were cut into 100-μm to maintain the structures of local axons, **Supplementary Fig. 2a**) with a freezing microtome (CryoStar NX50 cryostat, Thermo Scientific, San Jose, CA). All brain slices were stored in a 24-well plate with PBS, and representative slices with labeled neurons in the injection site and long-range projections away from the injection site were identified with a Slide-scanning Microscope (Nikon Ni-E, Japan) for further analysis.

Immunohistochemistry. Brain slices at the injection site of $cslAAV^{20,000}$-labeled ChAT-Cre transgenic mice (**Fig. 3c** and **Supplementary Fig. 7**) were selected for immunostaining. The following antibodies, including primary antibody, goat anti-choline acetyltransferase (Millipore, ab144p, 1:200) and secondary antibody, rabbit anti-Goat cy3 (Jackson Immunoresearch, 305-165-003, 1:500) were used in this study. Breifly, the selected 50-μm floating sections were initially blocked in 10% rabbit serum in PBS with 0.3% Triton X-100 (PBST) for 1 h at 37℃ and then washed with 0.3% PBST 10 min three times. Subsequently, sections were incubated in corresponding primary antibodies at 4℃ for 48-72 h followed by washes with 0.3% PBST 10 min three times and incubation in corresponding secondary antibodies at room temperature for 2 h.

Image Acquisition. All brain slices were counterstained with 4′,6-diamidino-2-phenylindole (DAPI) to determine the cortical and laminar borders, coverslipped with Anti-fade Fluorescence Mounting Medium (Beyotime Biotechnology, China) and sealed with nail polish for imaging.

To quantify the whole-brain direct input neurons (**Fig. 4**, **Supplementary Fig. 14** and **Supplementary Table 3**), all coronal sections throughout ten brains labeled by MAP-ENVIVIDERS and classical rAAV-RV system were obtained through Nikon

VS120 (Japan) with two (one for DAPI, one for DsRed) or three channels (the third for EGFP in injection site).

Except for images for input cells counting, all the other fluorescent images presented were acquired with a confocal laser scanning microscope (LSM710; Carl Zeiss, Germany) equipped with 405/488/514/561/633 excitation laser lines. 10x objectives (NA0.5) with a step size of 2 μm, 20x (NA0.8) with a step size of 1 μm, and 40x oil (NA1.4) with a step size of 0.39 μm were used. Generally, whole coronal sections containing the injection site were acquired at 10x (NA0.5) with a zoom of 1 or at 20x (NA0.8) with a zoom of 0.6. Regions of labeled somas were imaged and obtained in z-stacks with 10x (step size: 2 μm) or 20x objectives (step size: 1 μm). To obtain fine structures such as dendrite and axonal arborizations, 40x oil (step size: 0.39 μm) with a zoom of 1 was used for most images except for proximal spines of CA3 pyramidal neurons, where a zoom of 2 or 3 with the same objective was used (**Supplementary Fig. 5d**).

To faithfully compare the signal intensities among different labeling conditions (single virus vs. mixed viruses, littermate vs. stranger mixture, and littermate mixture vs. Thy1-EYFP-H line transgenic mice), parameters were adjusted low enough to ensure the fluorescent signal unsaturated, and then the same set of parameters was applied to all samples. The acquired z-stacks were stored in 16-bit depth TIFF format.

Resin Embedding. For whole-brain imaging with the TDI-fMOST system, a $lAAV^{200,000}$-labeled MOp mouse sample and a $cslAAV^{20,000}$-labeled basal forebrain mouse sample were embedded with Echnovit 9100 Methyl Methacrylate (MMA, Electron Microscopy Sciences, USA) according to previous procedures with minor optimizations[59]. Briefly, the removed PFA postfixed mouse brains were first rinsed in 0.01 M PBS for 12 h followed by complete dehydration in a series of alcohol (50%, 75%, 95%, 100%, and 100% ethanol, 2 h for each) and then xylene solution (twice, 2 h for each) for transparentization. The transparent brain was treated with sequential infiltration solutions (50%, 75%, 100%, and 100% resin in 100% ethanol, 2 h each for the first three solutions and 48 h for the final solution). Finally, the infiltrated brain was placed into a gelatin capsule filled with polymerization solution and kept in a dry chamber at -4°C in the dark for 72 h for polymerization before whole-brain sectioning.

Dual-color, whole-brain imaging with the TDI-fMOST system. Brain-wide images of the embedded mouse brain were acquired with the TDI-fMOST system at a voxel

size of 0.176 × 0.176 ×1 μm^3 (unpublished data)[36]. Dual-color, whole-brain imaging with real-time propidium iodide (PI) staining was performed as previously described[60]. The embedded mouse brain was immersed in 0.05 M Na_2CO_3 solution to enhance the EYFP signal and decrease the fluorescence background during the process of imaging and sectioning[59]. A 60x water-immersed objective (NA 1.0) was used to image the surface layer of the brain sample with an axial step size of 1 μm each cycle prior to sectioning with a diamond knife. Each coronal section was acquired with 16-bit and 8-bit depth for the green and PI channels, respectively. After ten to twelve days of uninterrupted imaging and sectioning, we eventually obtained whole-brain raw data with a total of 12,841 continuous coronal sections for the MOp brain sample (70.2 TB with 46.4 TB for green and 23.8 TB for red channels) and 10,781 continuous coronal sections for the BF brain sample (54.7 TB with 36.8 TB for green and 17.9 TB red channels), respectively.

Image processing. Raw data acquired with the dual-color TDI-fMOST system were preprocessed based on reported methods[60], including seamless stitch and image registration for two channels. The preprocessed images were stored in an LZW compression TIFF format, with 16-bit depth for the green channel and 8-bit depth for the PI channel. For the generation of 3D reconstructions of brain-wide long-range projections of the MOp and basal forebrain mouse sample, we selected 12,740 and 10,780 continuous coronal sections from the respective green-channel data set and resampled to 2 × 2 × 4 μm^3 before loading them into the Amira software (Visage Software, San Diego, CA). For the presentation of the MOp whole-brain dataset (**Supplementary Fig. 9**), coronal sections with maximum intensity projections (**Supplementary Fig. 9a-m**) were resampled to 0.6 × 0.6 μm^2 due to the large image size, and images to display fine structures, including somas, axonal branches and axonal arborizations (residual images in **Supplementary Fig. 9**) were all selected from corresponding coronal sections of original resolution (0.176 × 0.176 μm^2).

Raw data acquired with Nikon VS120 for whole-brain cell counting of input networks were transformed into JPG formats suitable for the following analysis. All confocal images were stored in lossless TIFF format. Image processing, including maximum intensity projection of serial z-stacks, adjusting brightness, and contrast of the composite images and selection of regions of interest, were performed with ImageJ (National Institutes of Health, USA). In addition, images imported from the Amira software were also processed as mentioned.

Morphology reconstructions of individual neurons in MOp and BF. These reconstructions were performed in the Filament Editor module of the Amira software (Mercury Computer Systems, San Diego, CA, USA) via a human-machine interaction pattern. For the reconstructions of neurons 1-8, we randomly chose two neurons in L2, one neuron in L3, one neuron in L6a and four neurons in L5b and started neuronal tracing from the soma. We first traced local axons projecting from the main axons, followed by the tracing of main axons projecting to contralateral parts or subcortical regions. For the reconstructions of neurons s1-s3, we selected axons in the anterior commissure (ac) as a start point and traced in two opposite directions, with one towards the ipsilateral part and the other towards the contralateral part. For the reconstructions of neurons c1-c3, we selected complex axonal arborizations in the ipsilateral lateral visual area (VISl) and caudoputamen (CP) and contralateral hippocampus as the start point and traced retrogradely. Because the axonal arborizations of most neurons were extremely complex and intermingled with each other, we made detailed registrations of the number and projection directions of all the branches to avoid negligence. For better differentiation, each part of the neuron, including the local axons, ipsilateral branches, and contralateral branches, were reconstructed separately. A constant $1000 \times 1000 \times 400\ \mu m^3$ data block was imported into the Amira software in each cycle of tracing. After complete reconstructions of all arborizations of one branch, we moved to the next branch and repeated the tracing steps until all the branches projecting from the main axons were reconstructed. During the process of tracing, two tracing modules, thin structure and linear options were used alternatively according to the sparseness of the axonal projections. For example, if the axonal projections were sparse and not interfered by other axons, the thin structure module was used to depict the axonal projection path from the start point to the end; otherwise, the linear module was utilized to gradually trace the path. The brightness and thickness of the data block were adjusted from time to time in the process of tracing based on the different conditions of the axonal projections. The dendrite morphologies of all neurons were reconstructed in the same way as axonal tracing but separately for convenient subsequent analysis. The tracing results for each neuron, including the axonal projections and dendrite morphologies, were rechecked by different skilled technicians, and neurons with uncertainties were excluded from the final results. The locations of nuclei were based on the Allen Brain Atlas (http://mouse.brain-map.org/static/atlas) with the aid of PI-staining signals.

Statistical analysis. Measurements of the signal profile (**Figs. 1a**,**b**,**e** and **Supplementary Figs. 1d,4b**) and relative fluorescence intensity (**Figs. 1c**,**2d**,**e**,**4d**,**f** and **Supplementary Figs. 1a-c**) were based on previously published methods with ImageJ[27]. Briefly, the signal profile of each pixel was calculated by subtracting the total signal value from the mean gray value of the background. We first measured the total signal value by a straight line drawn across the signal area (somas in the injection site or long-range axons) followed by measuring the mean gray value of the background by another straight line drawn across the background area close to the signal spot. For the measurement of relative fluorescence intensity, a rectangular selection (white dashed boxes) covering the signal spot (neuronal cell bodies) was made followed by the recording of the area of the boxes and the integrated density (IntDen) of the signal. To calculate the mean background, a straight line (yellow lines) was drawn across the background area close to the signal spot, and the mean gray value of the background was measured. The relative fluorescence intensity of each pixel was calculated by the relative signal values (resulting from subtraction of the total signal value from the total gray value of the background) over the pixel number of the area. For comparisons of signal intensity of EYFP and mCherry (**Fig. 1c**), 90 neurons from brain slices of the injection site were selected randomly from 3 independent experimental mice for the sAAV-EYFP/mCherry, rAAV2/9-EF1α-EYFP/PBS mixture (ratio of 1:1) and rAAV2/9-EF1α-mCherry/PBS mixture (ratio of 1:1). For comparisons of the signal intensity of sparsely labeled neurons (**Fig. 2d**,**e** and **Supplementary Fig. 1a**,**c**), 40 neurons from the brain slice of the injection site were selected randomly from three independent experimental mice for $lAAV^{20,000}$, $lAAV^{200,000}$, $sAAV^{20,000}$, $sAAV^{40,000}$ and $sAAV^{80,000}$, and 20 out of 24 neurons were selected from $lAAV^{1,000,000,}$ and 17 out of 26 neurons were selected from $sAAV^{1,000,000}$ (the other 9 neurons were hardly captured under low imaging parameters). As comparisons, 40 neurons of MOp, CA1 and CA3 regions were selected randomly from brain slices with similar bregma with lAAVs from Thy1-EYFP-H transgenic mice. For comparisons of the signal intensity of EYFP and mCherry in starter cells within the lAAV-DIO-GT/RG- and sAAV-DIO-GT/RG labeling groups (**Fig. 4d** and **Supplementary Fig. 1b** left), a total of 170 neurons were selected randomly from 3 independent experimental mice for both groups. For comparisons of the signal intensity of mCherry in input cells within the lAAV-DIO-GT/RG- and sAAV-DIO-GT/RG labeling groups (**Fig. 4f** and **Supplementary Fig. 1b** right), 160 neurons for

RT, 190 neurons for SSp and SSs were selected randomly from 3 independent experimental mice for both groups.

Whole-brain counting of input cells was performed following previously published methods[45,46]. Briefly, input cells in each coronal section were identified manually, followed by registration of each coronal section to the Allen Brain Atlas (ABA, http://mouse.brain-map.org/). We summed the total number of input neurons and calculated the convergent index (ratio between input cells and starter cells)[18] in diverse gross regions and subregions. For the demonstration of relationship between proportion of inputs and enhanced ratios of tracing efficiency provided by MAP-ENVIVIDERS (**Fig. 4g**), we calculated selected 44 representative subregions from 11 major regions from sAAV-DIO-GT/RG labeling groups and calculated proportion of inputs, i.e. inputs in these subregions against total inputs (for better demonstration, proportion of inputs in x-axis were listed by logarithm to base 10, denoted by lg %). Enhanced ratios of tracing efficiency provided by MAP-ENVIVIDERS (y-axis) were denoted by convergent index of lAAV-DIO-GT/RG dividing by convergent index of sAAV-DIO-GT/RG in diverse subregions.

All quantitative data, including cell numbers and measurement of relative signal intensity, convergent index and proportion of inputs, were all presented as the mean ± s.e.m. Significance was analyzed using one-way ANOVA with Dunnett's post hoc test (**Fig. 2d**), Student's t-test (**Figs. 1c**,**f**,**2e,4d,f**) and Mann-Whitney U test (**Supplementary Fig. 14**) in GraphPad Prism version 6.0 (GraphPad Software Inc., San Diego, CA, USA).

The reconstructed axons and dendrites of neurons s1-s3 and c1-c3 were saved in SWC files for the quantitative analysis of the branches and length in the software Neurolucida Explorer (MicroBrightField, USA).

Supplementary Information

Supplementary Figure 1

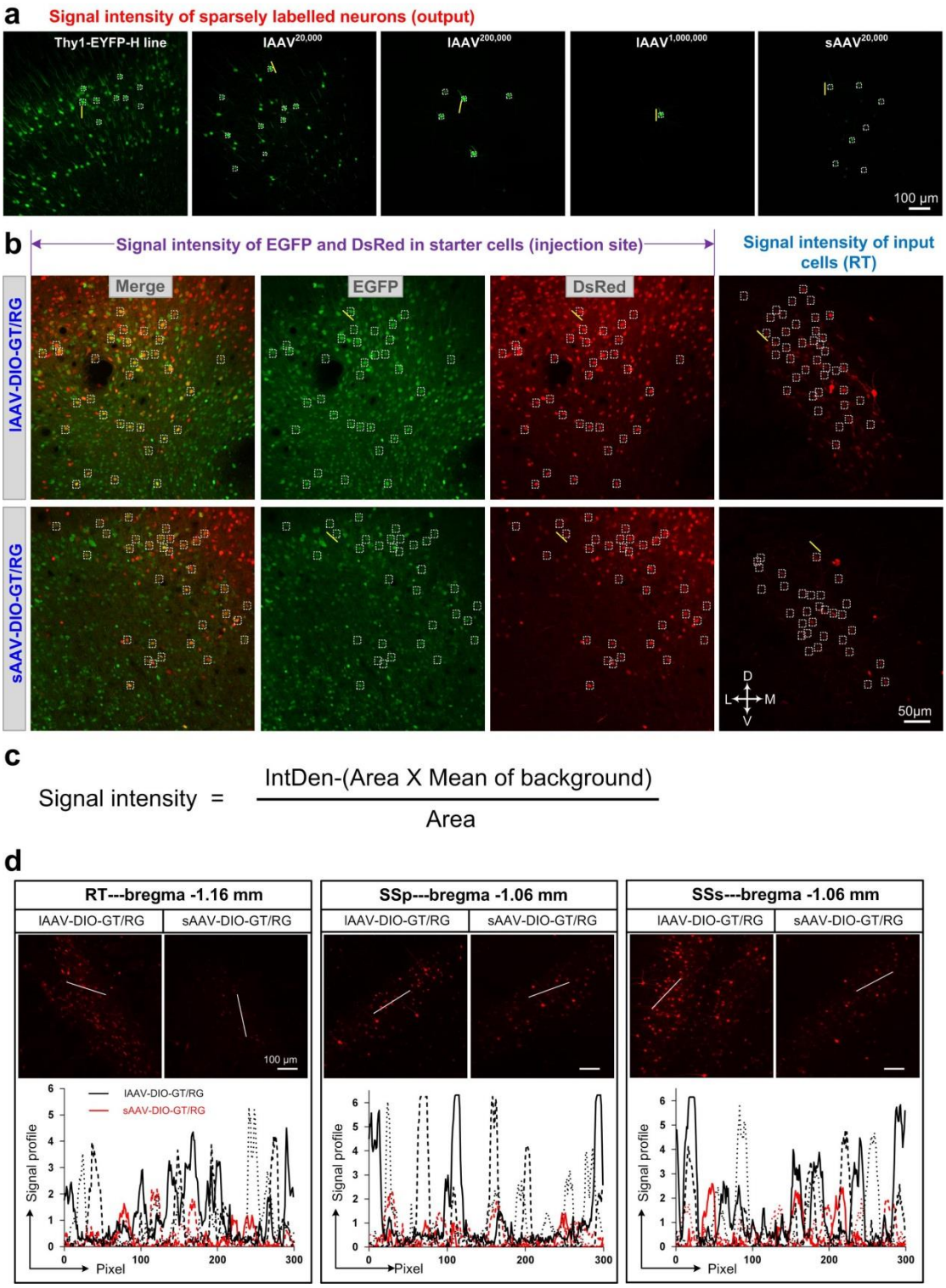

Supplementary figure 1

Schematic of measuring fluorescence intensity and Signal profile of individual neurons.

(a-c) Schematic of measuring fluorescence intensity of individual neurons.

(a) Representative confocal images showing the measurement of signal intensity of neurons in Thy1-EYFP-H line transgenic mice and sparsely labeled neurons with diverse lAAVs and sAAVs in MOp region.

(b) Representative confocal images showing the measurement of signal intensity of EGFP and DsRed in starter cells and DsRed-labeled input cells in lAAV-DIO-GT/RG- and sAAV-DIO-GT/RG-treated mice. All of the images were obtained under the same imaging conditions (low laser intensity was used to avoid over-exposure of the cell bodies).

(c) The signal intensities were calculated in ImageJ according to the formula in **c** and the method in the previous report[27]. Briefly, a rectangular selection (white dashed boxes) covering the signal spot (neuronal cell bodies) was made, and then the area of the boxes and the integrated density (IntDen) of the signal were recorded. To calculate the mean background, a straight line (yellow lines) was drawn across the background area close to the signal spot and the mean gray value of the background was measured. This method was applied to calculate the signal intensities in Fig 2d,e and Fig. 4d, f.

(d) Signal profile of input neurons in RT, SSp and SSs in lAAV-DIO-GT/RG and sAAV-DIO-GT/RG labeling groups. n = 3 mice for each group. SSp, primary somatosensory area; SSs, supplemental somatosensory area.

Supplementary Figure 2

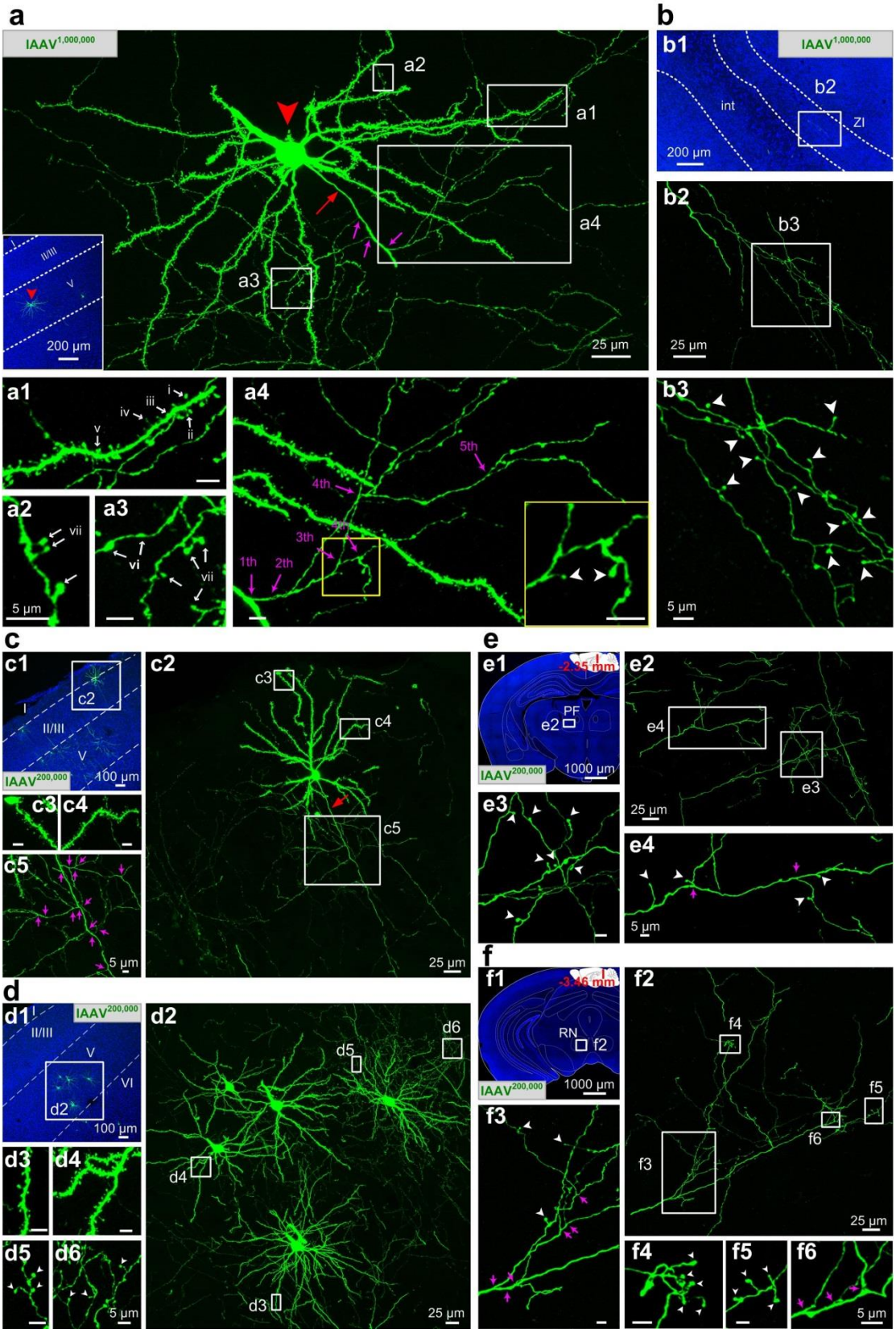

Supplementary figure 2

Fine structures of individual neurons labeled with lAAV^{1,000,000} and lAAV^{200,000}.

(a) Confocal image (100-μm thickness) of a representative individual neuron labelled with lAAV^{1,000,000} in injection site. Inset showed the localization of cell body (indicated by red arrowhead). **(a1)** Five types of spines: (i) mushroom, (ii) thin, (iii) stubby, (iv) filopodium, and (v) branched spines. **(a2-a3)** Two types of boutons: (vi) en passant boutons and (vii) terminal boutons. **(a4)** Different levels of local axonal collaterals.

(b) Confocal images of representative long-range axonal projections in the ZI region (**b1**) labelled with lAAV^{1,000,000}. Fine structures were progressively enlarged from **b1** to **b3**.

(c-d) Fine structures of MOp L2 (**c**) and L5 (**d**) pyramidal neurons labelled with lAAV^{200,000} in injection site. **c1** and **d1** were low-magnification images indicating the locations of cell bodies. **c2** and **d2** were high-magnification images showing the fine structures of the representative neurons. **c3-c5** and **d3-d6** were enlargements of box regions in **c2** and **d2**, respectively.

(e-f) Fine structures of MOp long-range axonal projections labelled with lAAV^{200,000}. **e1** and **f1** were composite coronal sections indicated the locations of the axonal projections, including parafascicular nucleus (PF, **e1**) in thalamus and red nucleus (RN, **f1**) in midbrain. **e2** and **f2** were high-magnification images showing the fine structures of the complex axonal arborizations. **e3-e4** and **f3-f6** were enlargements of the boxed regions in **e2** and **f2**, respectively. Red arrows indicated the primary axon emitting from soma. The pink arrows and numerals indicate the orders of the axonal branches and bright, large bulb-shaped terminal boutons were indicated by white arrowheads.

Definition the boundary of cortical layers (indicated by white dashed lines) and location of nuclei were all based on DAPI (4',6-diamidino-2-phenylindole, blue) staining. int, internal capsule; ZI, zona incerta. I-VI, cortical layers I to VI.

Supplementary Figure 3

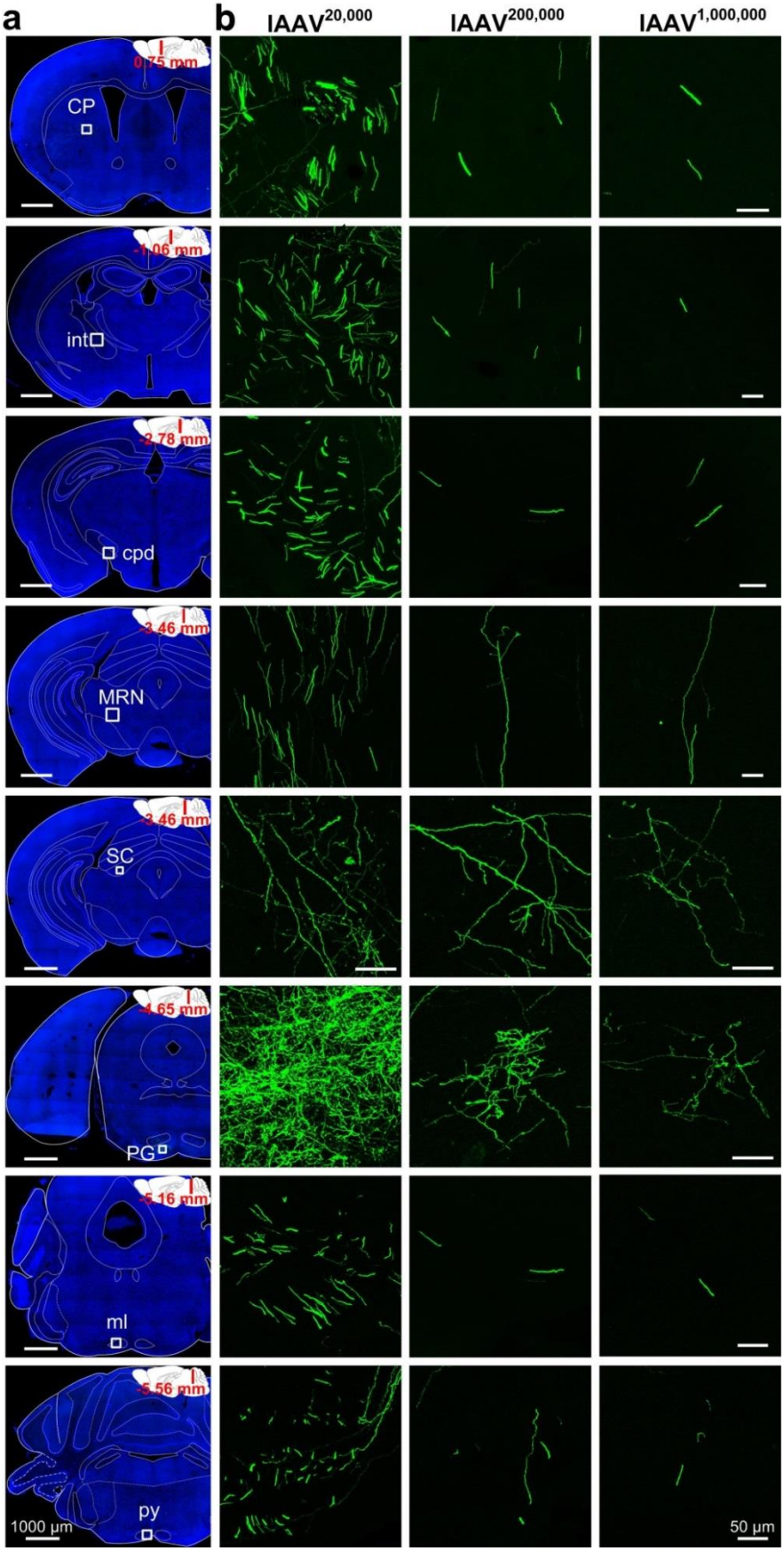

Supplementary figure 3

Brain-wide long-range axonal projections of three lAAVs in MOp.

We injected equal volume (100 nl) of three lAAVs ($lAAV^{20,000}$, $lAAV^{200,000}$ and $lAAV^{1,000,000}$) into MOp of wild-type mice. After 21d's expression, we examined brain-wide long-range axonal projections of three lAAVs, including CP (bregma level: 0.75 mm), int (bregma level: -1.06 mm), cpd (bregma level: -2.78 mm), MRN and SC (bregma level: -3.46 mm), PG (bregma level: -4.65 mm), ml (bregma level: -5.16 mm), and py (bregma level: -5.56 mm).

(a) Composite coronal sections showing the locations of the axonal projections.

(b) Maximum-intensity projections of the boxed regions in **a**, showing the fine structures of the axonal projections in different brain regions. Images coming from the same brain region were obtained with the same imaging conditions and processed identically.

Abbreviations: CP, caudoputamen; int, internal capsule; cpd, cerebal peduncle; MRN, midbrain reticular nucleus; SC, superior colliculus; PG, pontine gray; ml, medial lemniscus; py, pyramid.

Supplementary Figure 4

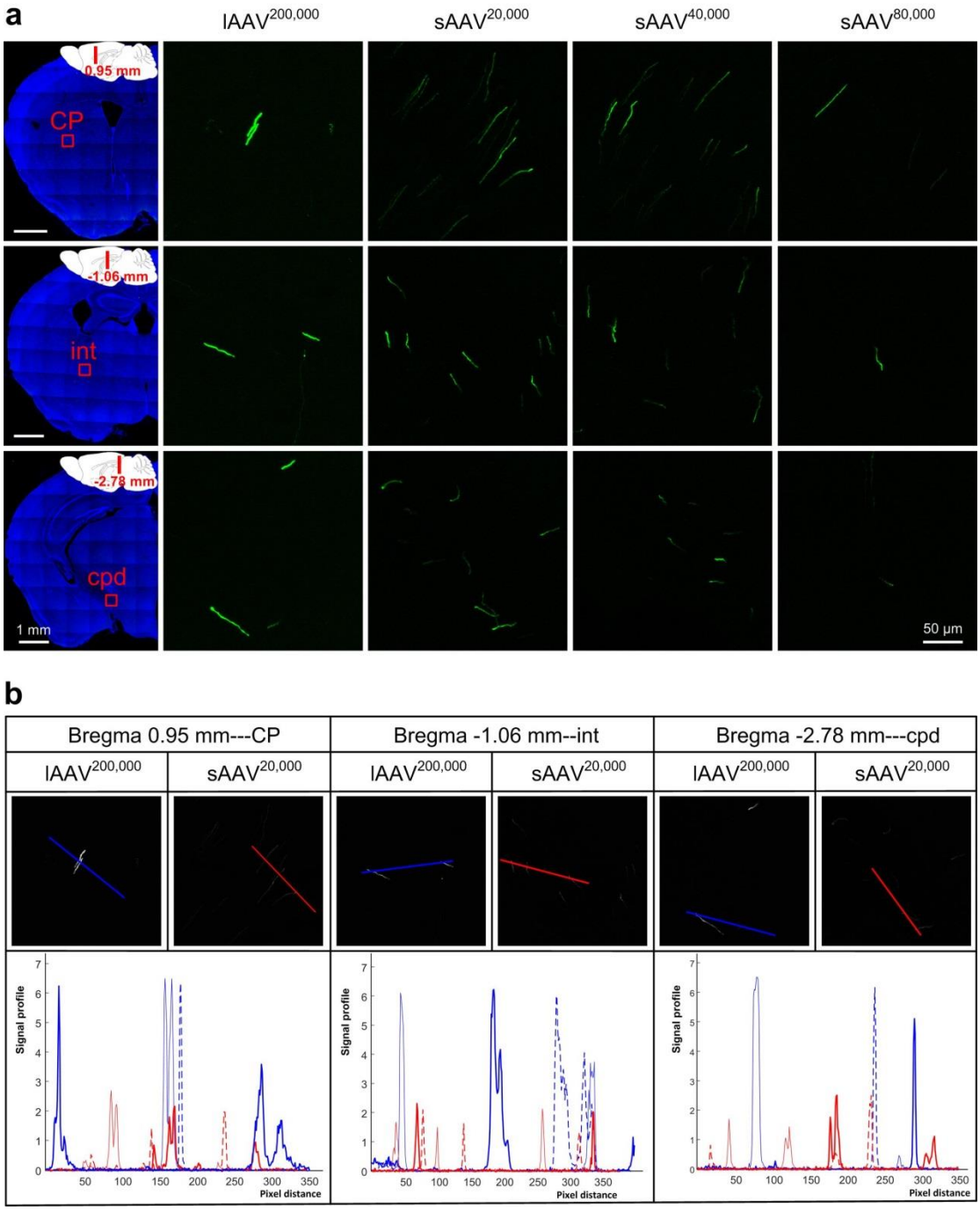

Supplementary figure 4

Comparisons of brightness of long-range axonal projections between lAAV^{200,000} and diverse sAAVs (sAAV^{20,000}, sAAV^{40,000} and sAAV^{80,000}).

(a) Representative confocal images of long-range axonal projections in different brain regions. All images in each brain region were obtained under the same imaging conditions and processed identically.

(b) Measurements of fluorescence intensities in **a** for $lAAV^{200,000}$ (indicated by blue lines, three types of blue lines represent three different mice) and $sAAV^{20,000}$ (indicated by red lines, three types of red lines represent three different mice). The data showed that the fluorescence in neurons labelled by lAAVs was stronger than by sAAVs.

Supplementary Figure 5

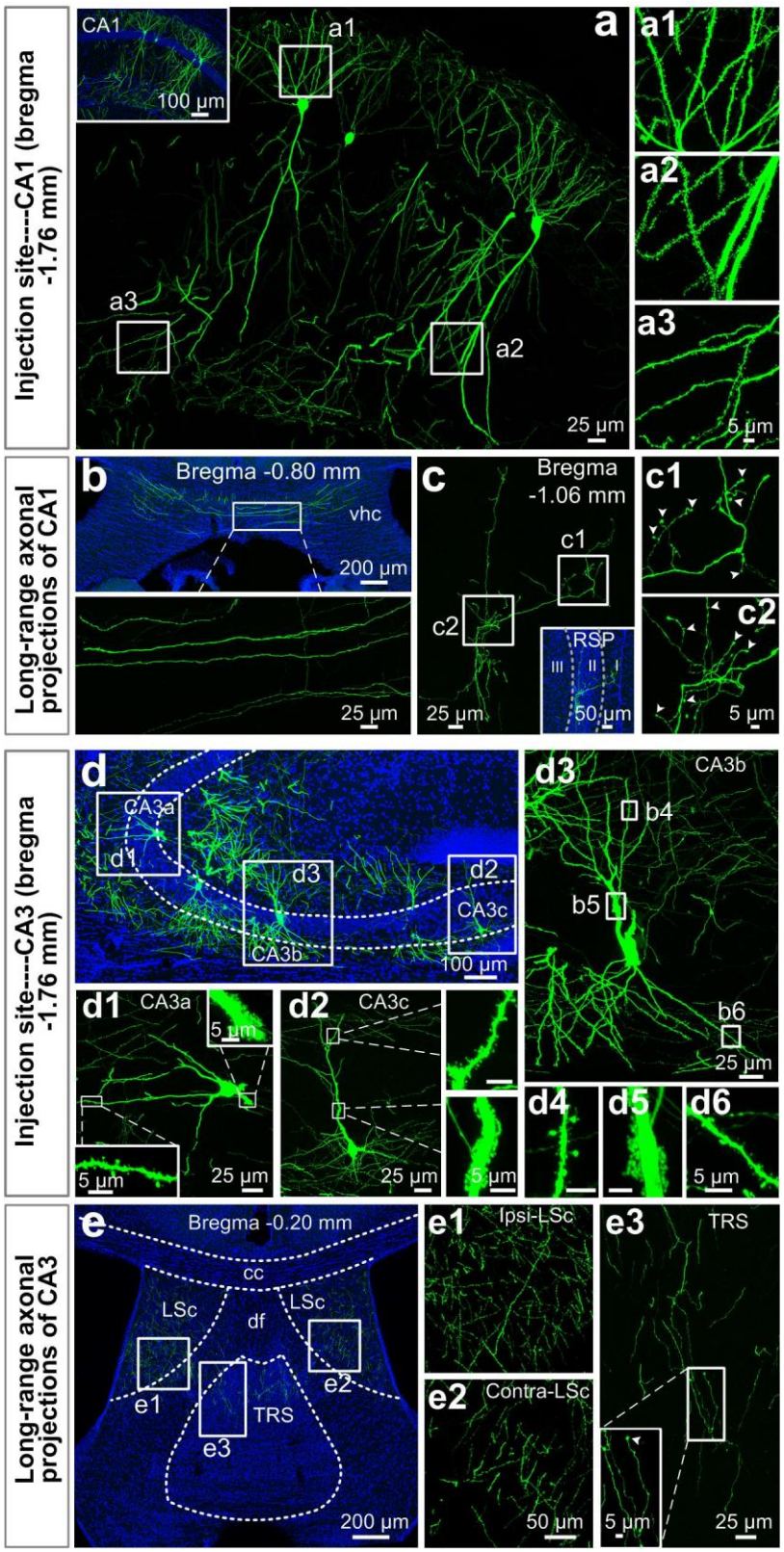

Supplementary figure 5

Applications of lAAV^{200,000} in CA1 and CA3 region.

(a-c) Applications of lAAV^{200,000} in CA1 region.

(a) Representative confocal images showing the fine structures of labelled neurons in injection site of CA1. Inset shows the locations of the somata.

(a1-a3) Enlargements of the boxed regions in **a** showing different parts of dendritic spines.

(b-c) Representative confocal images of the long-range axonal projections of CA1 in ventral hippocampal commissure (vhc, **b**) and retrosplenial cortex (RSP, **c**). **c1-c2** were enlargements of the corresponding boxed regions in **c**. Insets in **c** were approximate location of the axonal arborizations. White arrowheads indicate terminal boutons. White dashed lines on inset define the boundary of cortical layers based on DAPI staining.

(d-e) Applications of lAAV^{200,000} in CA3 region.

(d) Low-magnification images showing the overall labelling in CA3.

(d1-d3) Fine structures of the CA3a (**d1**), CA3b (**d3**), and CA3c (**d2**) pyramidal neurons. Respective box regions in **d1** and **d2** were enlarged to show proximal and distal dendritic spines.

(d4-d6) Enlargements of the box regions in **(d3)** showing apical **(d4),** proximal **(d5),** and basal dendritic spines **(d6)** of CA3b pyramidal neuron, respectively.

(e) Low-magnification images indicate the locations of the axonal projections in TS and LS. The location of nuclei was based on Paxinos Mouse Brain Atlas (PMBA) with the aid of DAPI staining. **(e1-e3)** High-magnification images of the boxed regions in **e** showing the fine structures of axonal projections and axonal terminals.

Abbreviations: CA1, field CA1 of hippocampus; CA3, field CA3 of hippocampus; DG, dentate gyrus; cc: corpus callosum; df: dorsal fornix; LSc: lateral septal nucleus, caudal (caudodorsal) part; TRS: triangular nucleus of septum.

Supplementary Figure 6

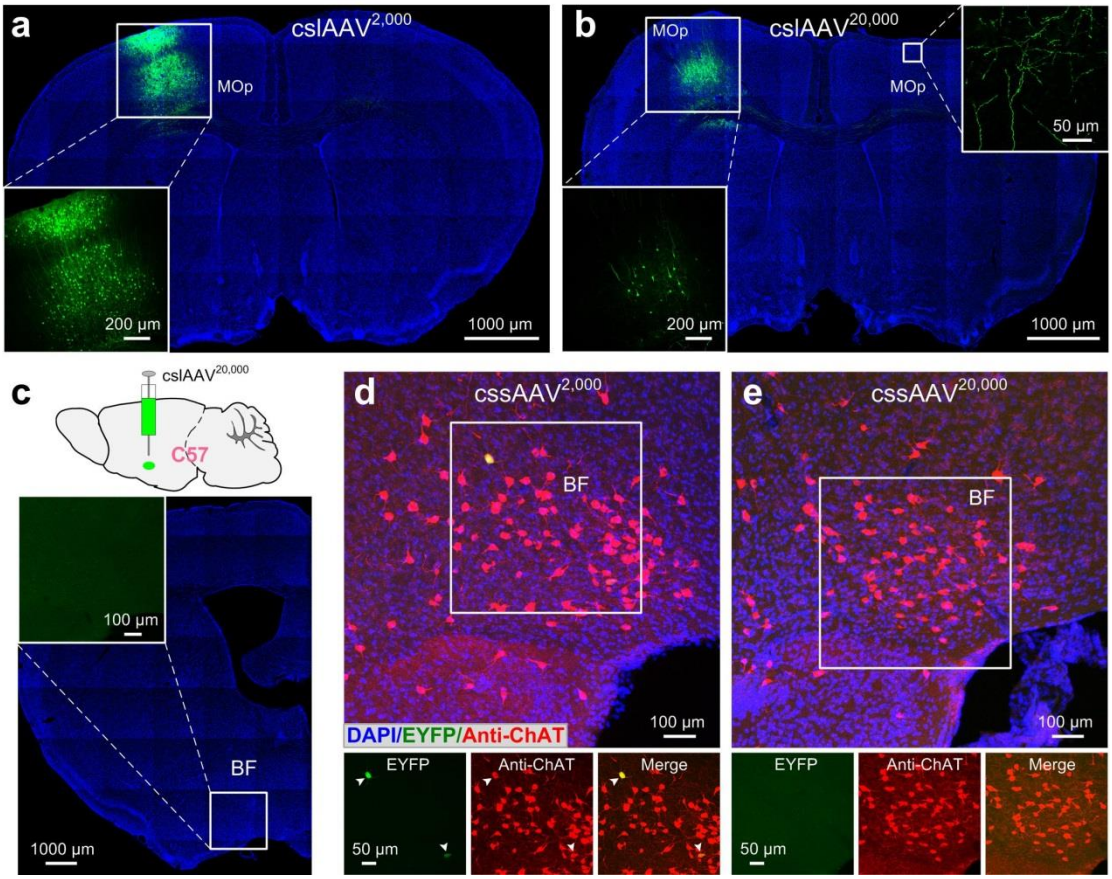

Supplementary figure 6

Validation of cell-type-specific labelling strategy with cslAAVs in Thy1-Cre and ChAT-Cre transgenic mice.

(a-b) Two versions of cslAAVs, cslAAV^{2,000} (**a**) or cslAAV^{20,000} (**b**) were injected into MOp of Thy1-Cre transgenic mice to achieve tunable neuron labeling. Lower left insets in **a** and **b** were enlargements of the corresponding boxes showing labeling in injection sites. Upper right inset in **b** was contralateral MOp axonal projections.

(c) 100nl cslAAV^{20,000} was injected into basal forebrain (BF) of wild-type mice, we found no neurons were labelled across the injection site of 4 injected mice 21d later, indicating that the expression of cslAAVs was strictly restricted to Cre-driver lines**.**

(d-e) For control experiments, we injected 100 nl two diluted ratios of Flp-expressing rAAV: Flp- and Cre-dependent rAAVs mixtures (abbreviated for cssAAV^{2,000} and cssAAV^{20,000} hereafter, in which the Flp-expressing rAAV was diluted to ratios of 1:2,000 and 1:20,000 in PBS respectively before equally mixed with Flp- and Cre-dependent rAAV into BF of ChAT-Cre transgenic mice (n=5 mice each). We found no labelled neurons were detectable in cssAAV^{20,000}-treated mice and in cssAAV^{2,000}-treated mice, only two mice each contained three or four faintly labelled cholinergic

neurons (note that the imaging parameters of EYFP were much higher than **Fig. 3c**) whereas the other three mice rarely contained any signals in injection sites.

Supplementary Figure 7

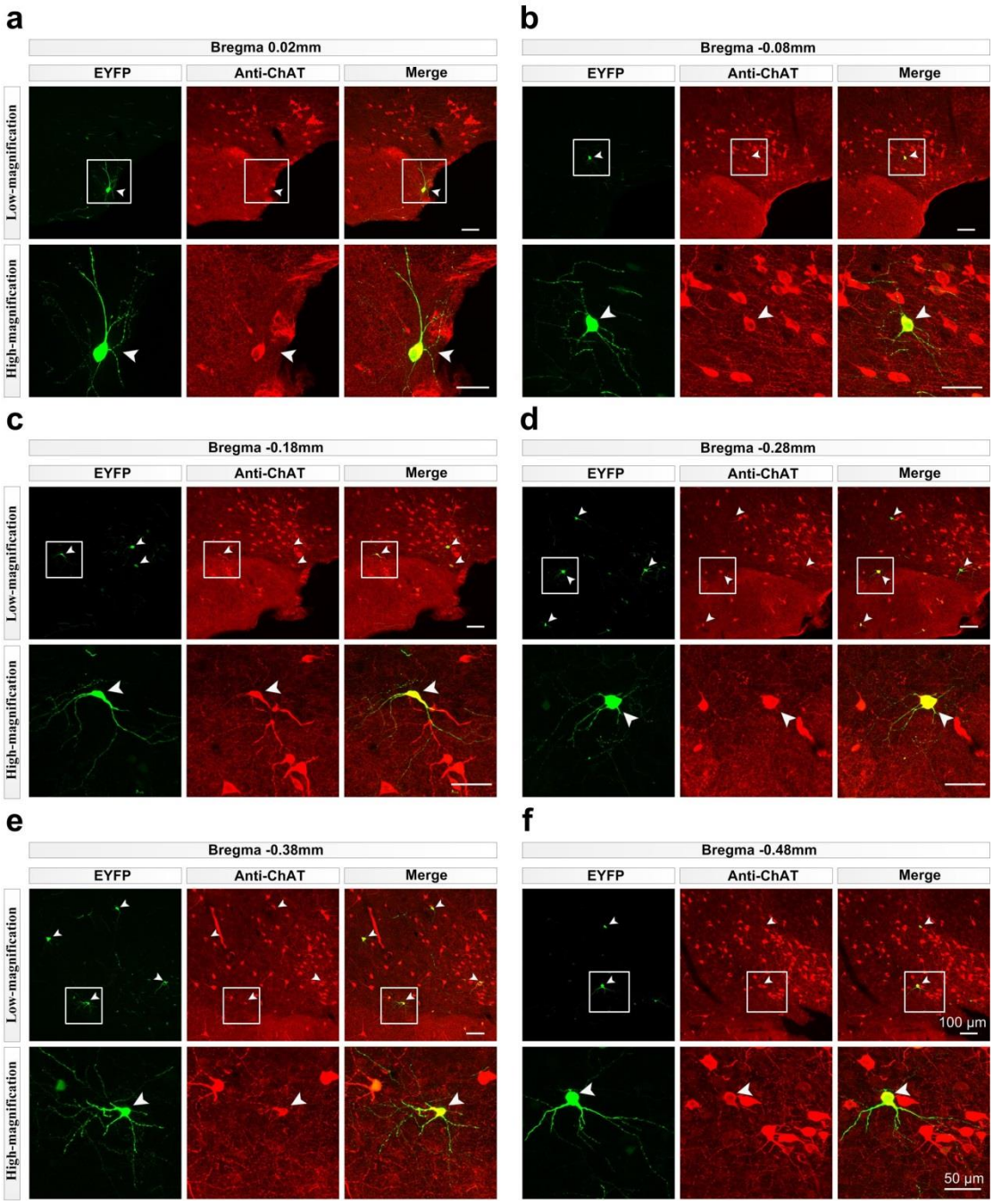

Supplementary Figure 7 (continued)**:**

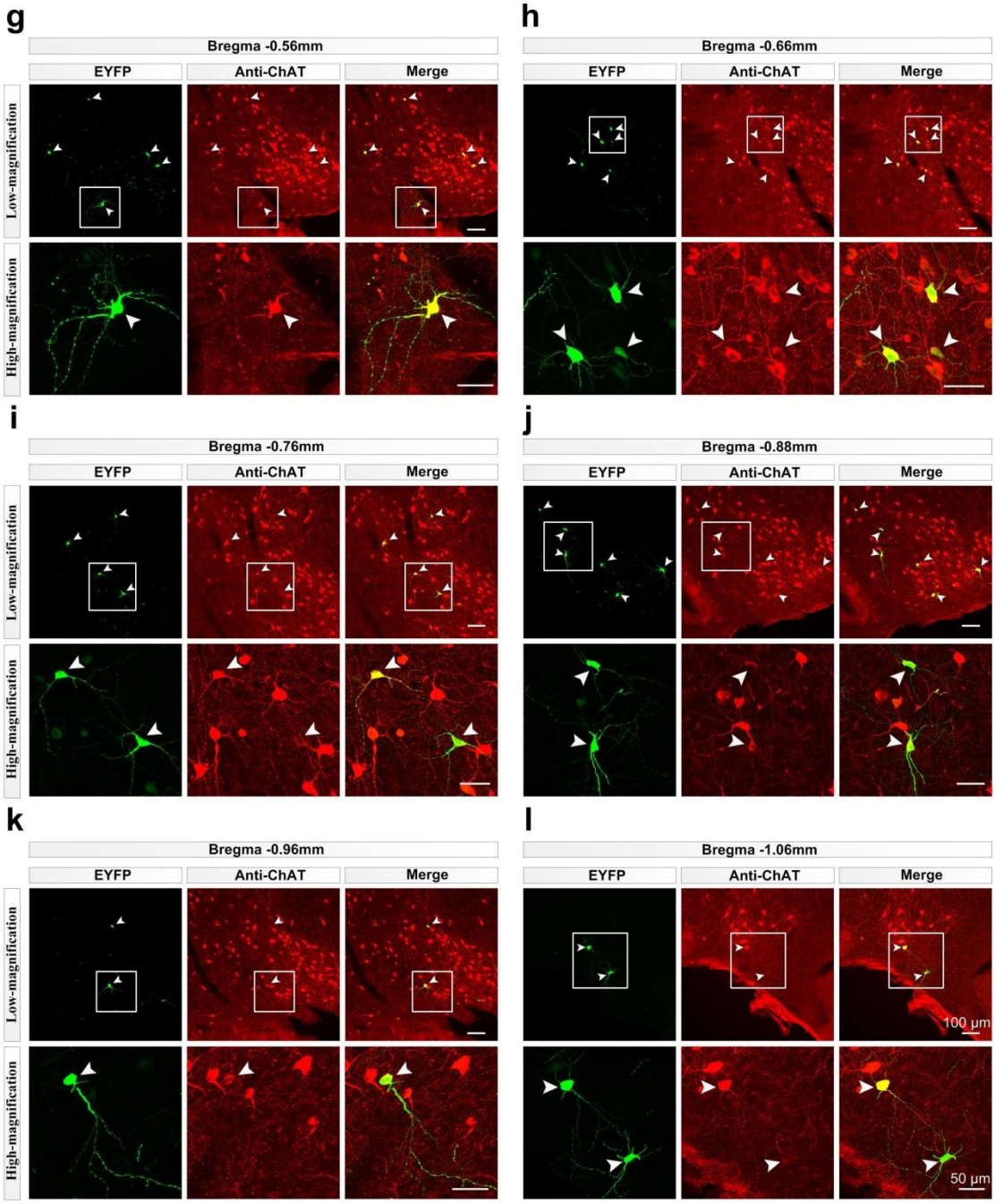

Supplementary figure 7

Cell-type-specific, sparse and suprebright BF cholinergic neuron labelling. Twelve 50-μm thickness coronal sections ranging from Bregma 0.02 mm to Bregma -1.06 mm of the injection site were selected from a cslAAV^{20,000}-labeled ChAT-Cre transgenic mouse sample and displayed with a 50-μm intervals and immunostained with anti-ChAT antibody. Upper panels of **a-l** were low-magnification images showing overall labelling on each section and lower panels were high-magnification images of the corresponding boxes. Colabelled neruons were indicated by white arrowheads. This brain sample contained 62 labelled neurons (mouse 4 in

Supplementary Table 1) and all of them were ChAT-positive and approximately 39 neurons were listed here.

Supplementary Figure 8

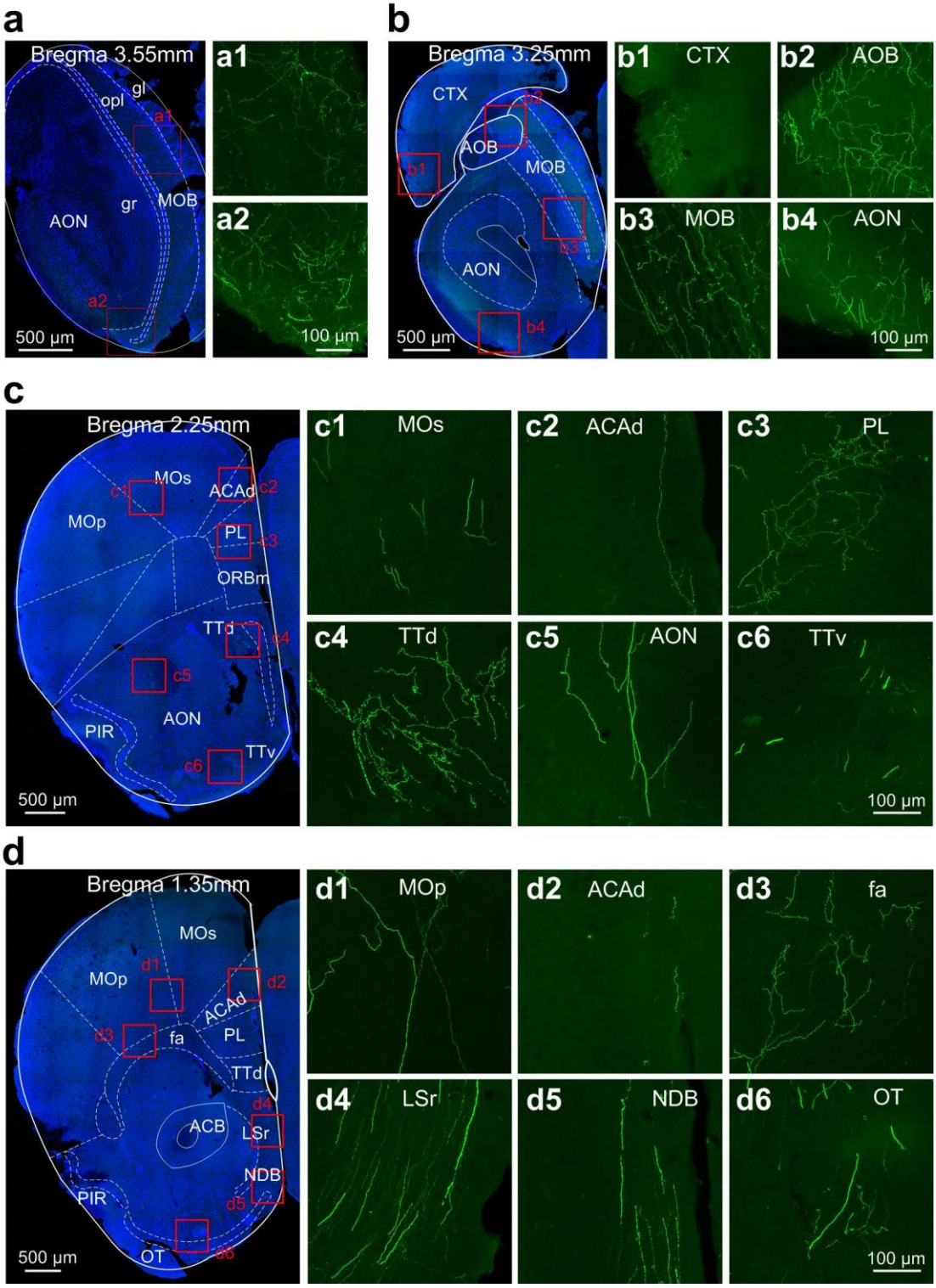

Supplementary Figure 8 (continued)**:**

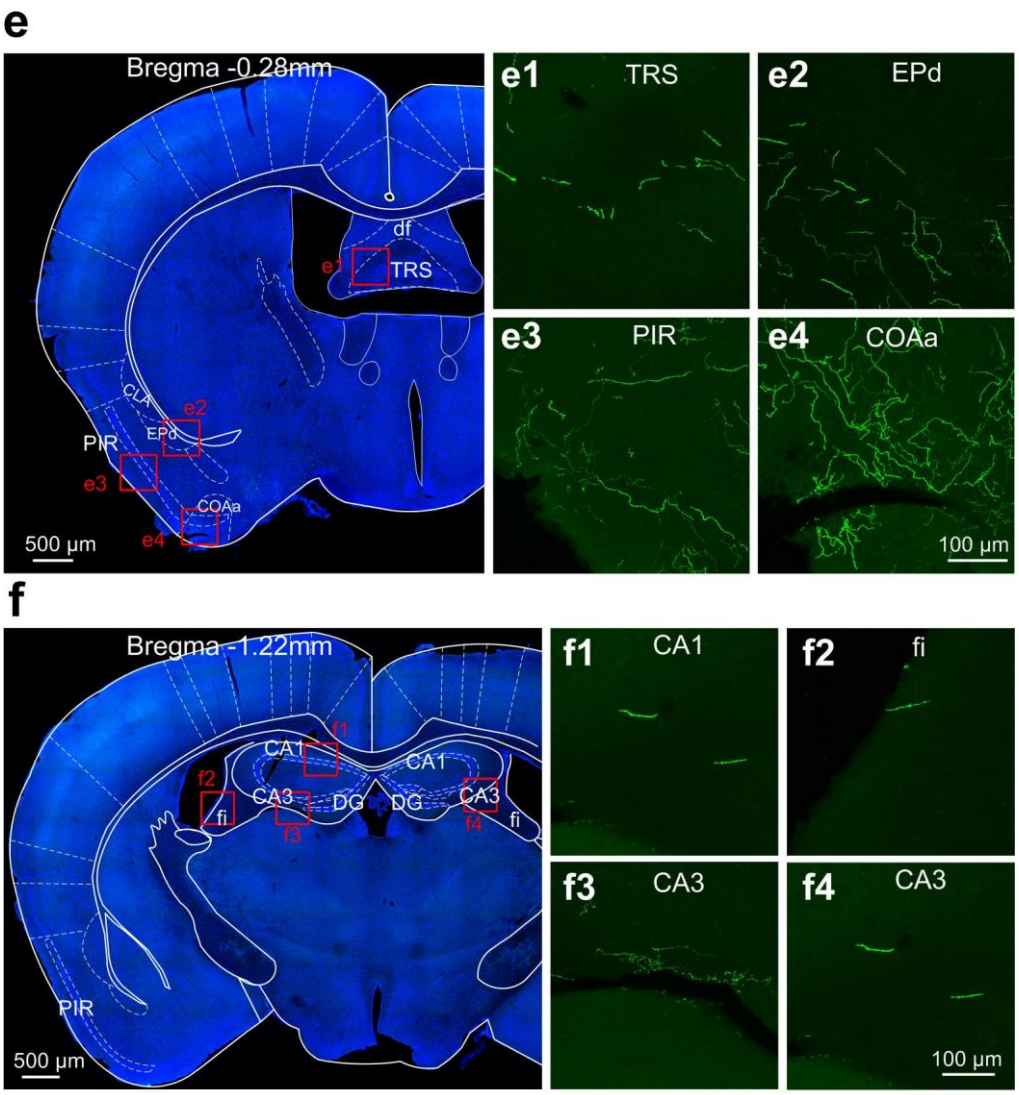

Supplementary figure 8

Brain-wide long-range projections of BF cholinergic neurons.

Five coronal sections from a representative cslAAV^{20,000}-labelled ChAT-Cre transgenic mouse brain sample were selected to show part of their main axonal projections. **a1-a2**, **b1-b4**, **c1-c6**, **d1-d6**, **e1-e4** and **f1-f4** were maximum-intensity projections of the respective boxed regions in **a-f** showing the details of the axonal projections in different brain regions.

Abbreviations: MOBgl, main olfactory bulb, glomerular layer; MOBopl, main olfactory bulb, outer plexiform layer; MOBgr, main olfactory bulb, granule layer; MOB, main olfactory bulb; AON, accessory olfactory nucleus; CTX, cerebral cortex; AOB, accessory olfactory bulb; MOp, primary motor area; MOs, secondary motor area; ACAd, Anterior cingulate area, dorsal part; PL, Prelimbic area; ORBm, Orbital area, medial part; TTd, taenia tecta, dorsal part; TTv, taenia tecta, ventral part; PIR,

piriform area; ACAd, anterior cingulate area, dorsal part; fa, fcorpus callosum, anterior forceps; ACB, nucleus accumbens; LSr, lateral septal nucleus, rostral (rostroventral) part; NDB, diagonal band nucleus; OT, olfactory tubercle; df, dorsal fornix; TRS, triangular nucleus of septum; CLA, claustrum; ENd, endopiriform nucleus, dorsal part; COAa, cortical amygdalar area, anterior part; CA1, field CA1 of hippocampus; CA3, field CA3 of hippocampus; DG, dentate gyrus; fi, fimbria of the hippocampus.

Supplementary Figure 9

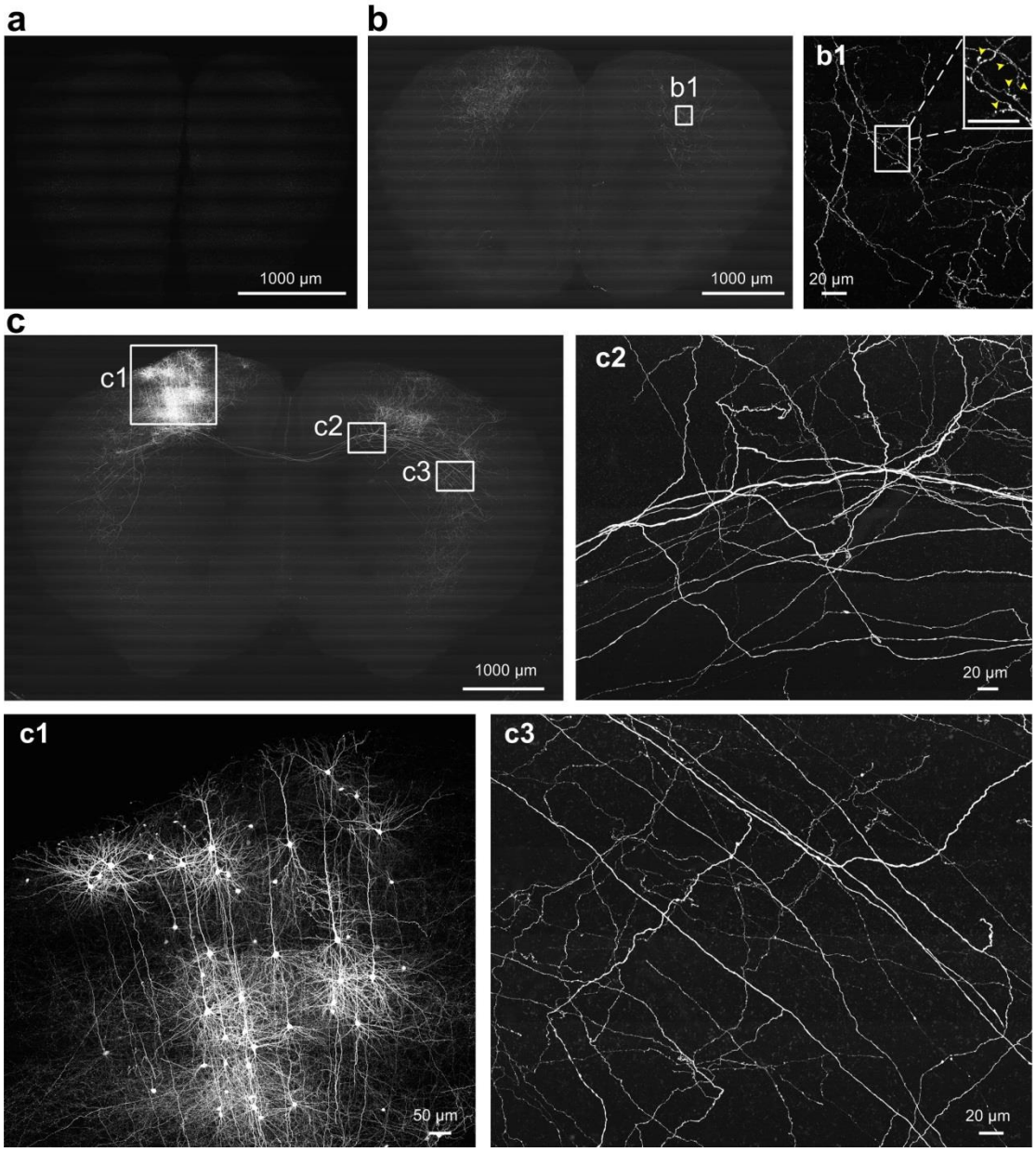

Supplementary Figure 9 (continued)**:**

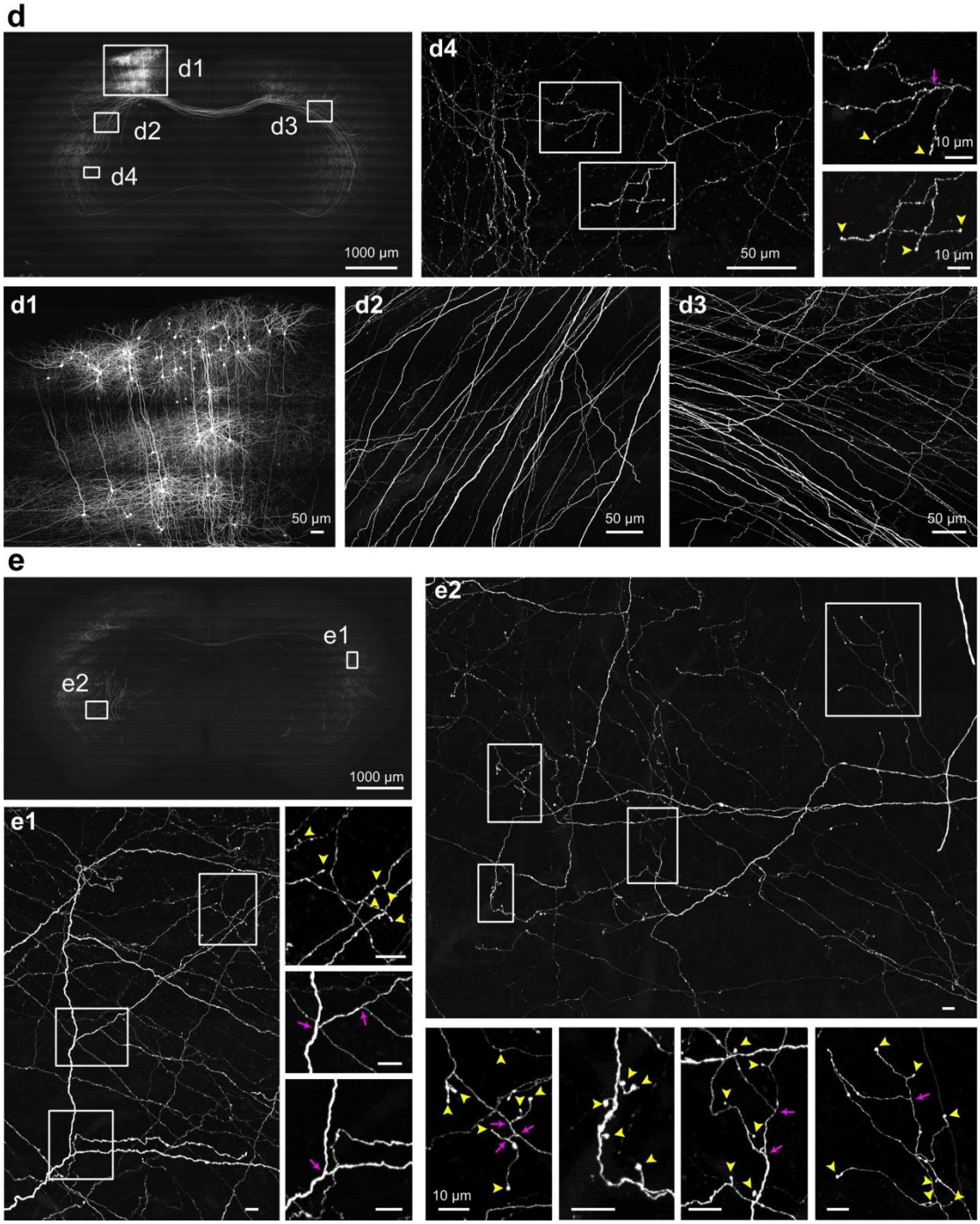

Supplementary Figure 9 (continued)**:**

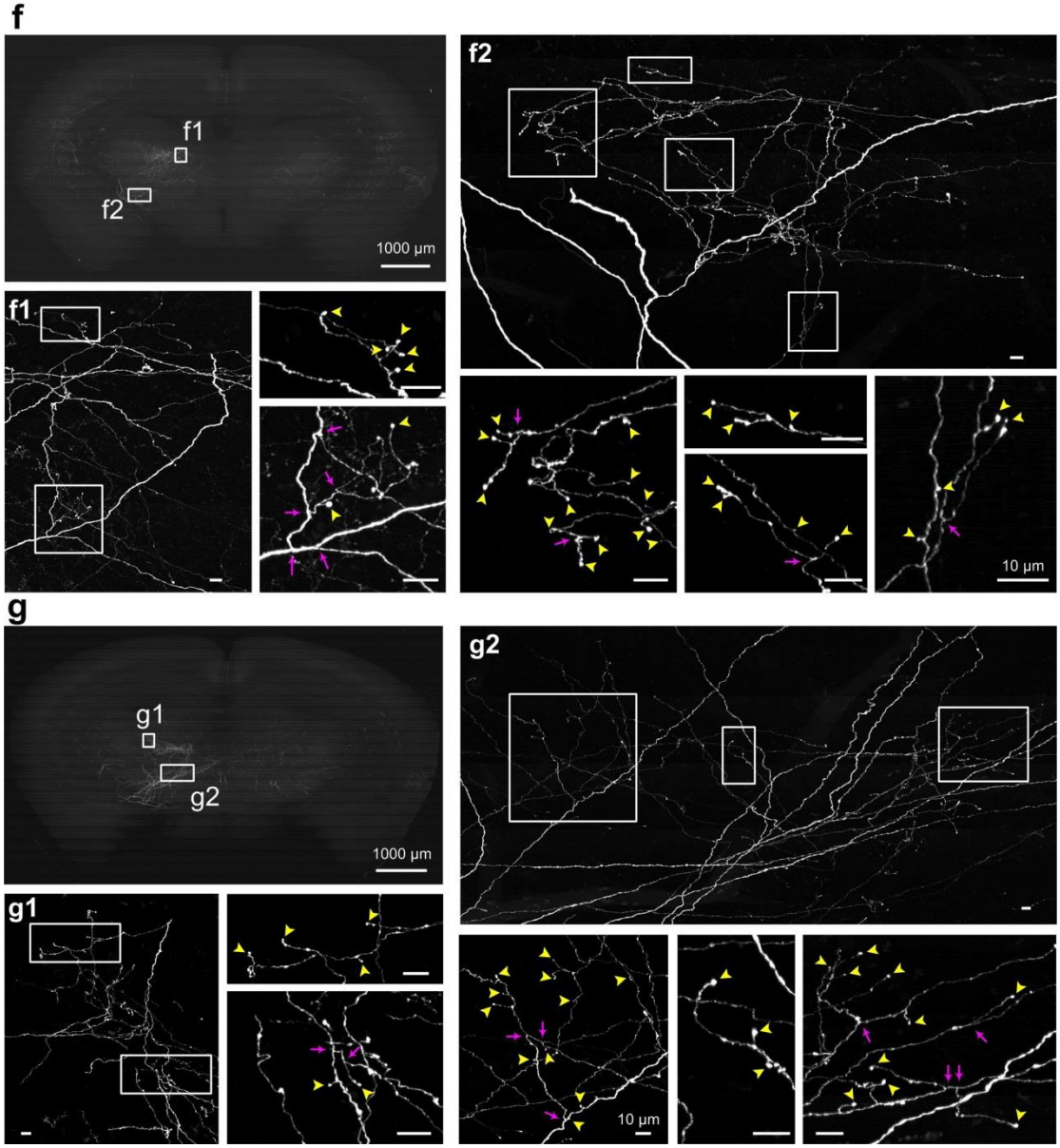

Supplementary Figure 9 (continued)**:**

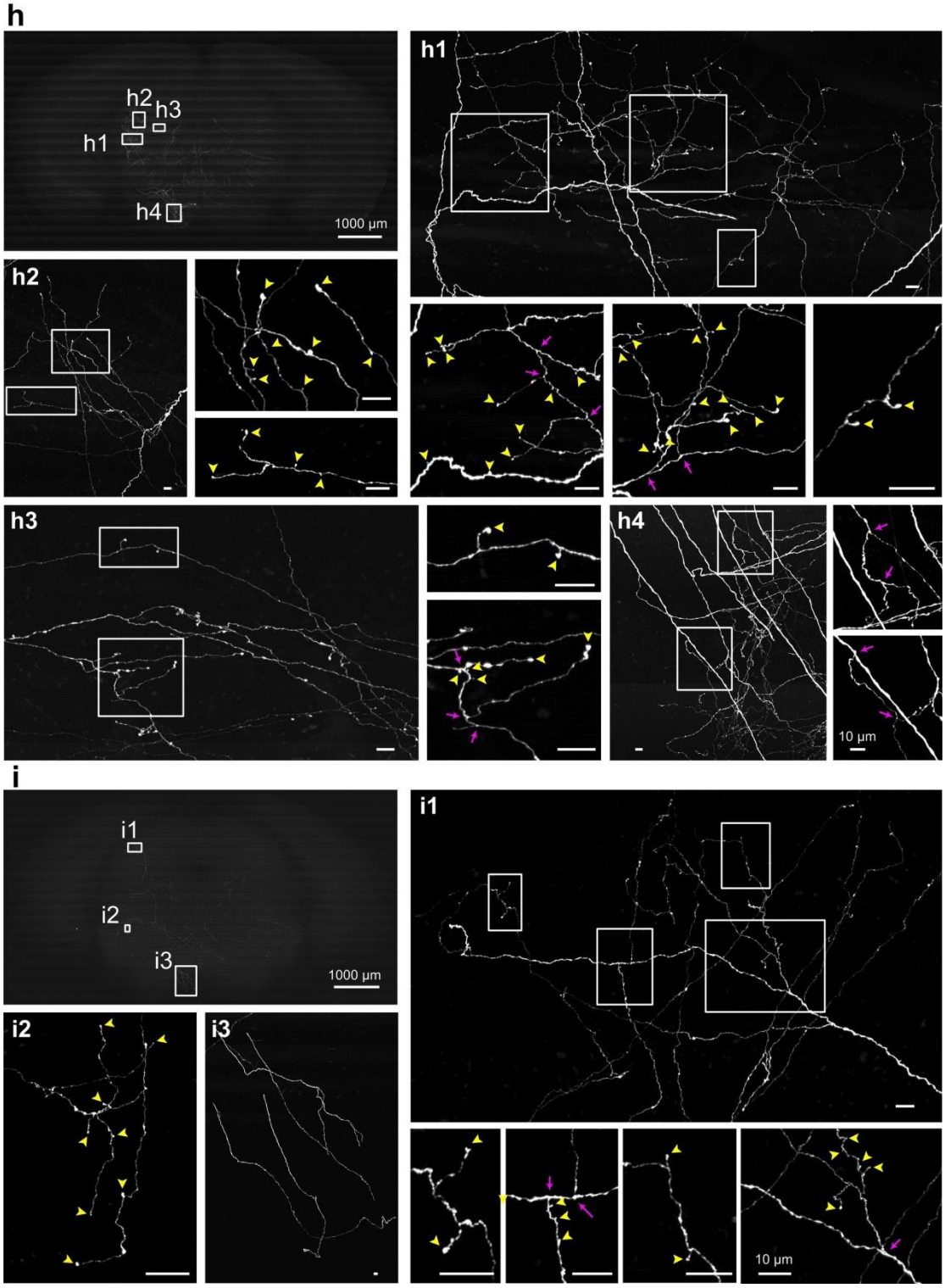

Supplementary Figure 9 (continued)**:**

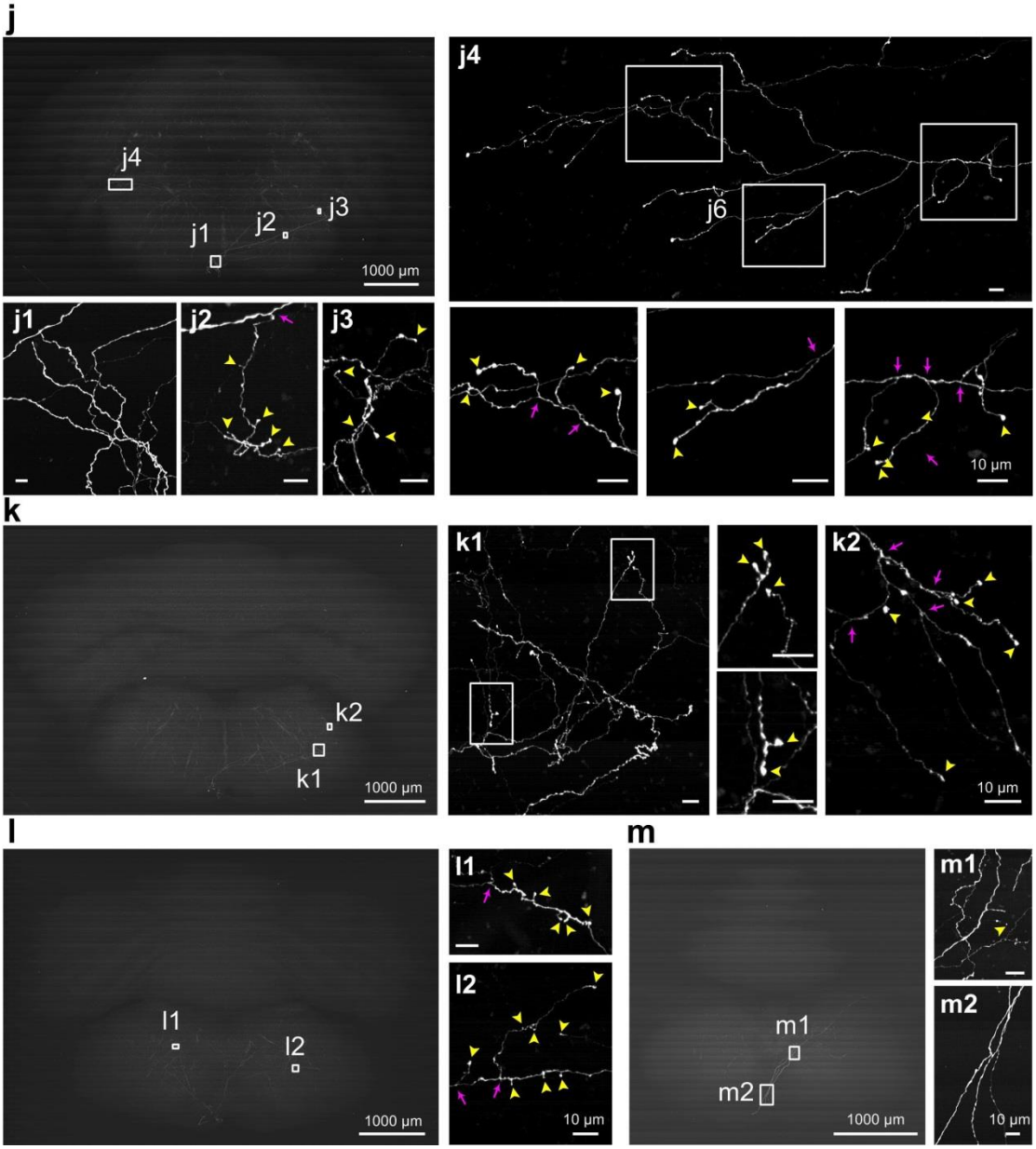

Supplementary figure 9

Whole-brain data sets of MOp (labelled with lAAV^{200,000}).

a and **b** were maximum-intensity projections of 800 and 1600 coronal sections. **c-l** were maximum-intensity projections of 1000 coronal sections and **m** was maximum-intensity projections of 420 coronal sections, respectively. All other images were enlargements of respective box regions showing the injection site or fine structures, including axonal branches (indicated by purple arrows) and terminal boutons (indicated by yellow arrowheads).

Supplementary Figure 10

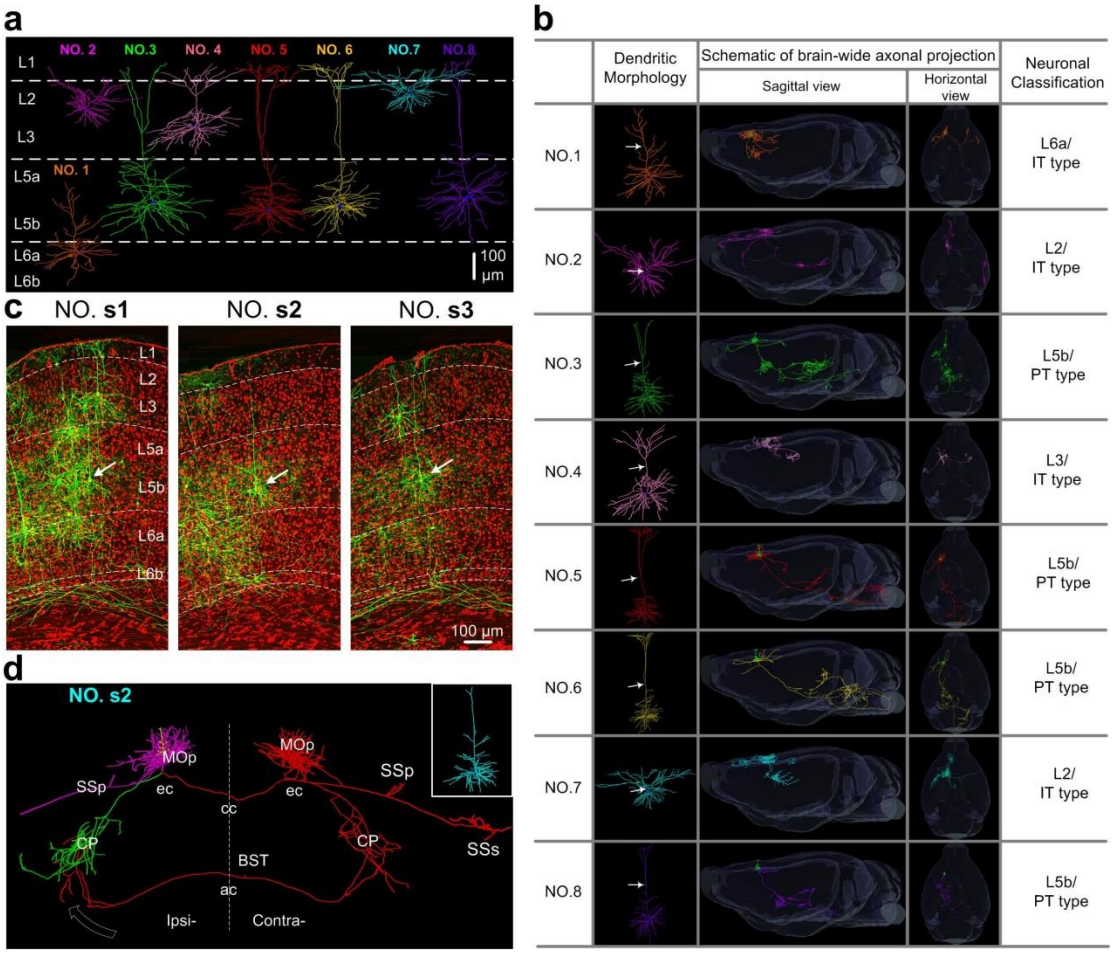

Supplementary figure 10

Localization, dendritic and axonal morphologies of the reconstructed MOp pyramidal neurons.

(a) Gallery of dendritic morphologies and approximate laminar distributions of eight reconstructed pyramidal neurons (No.1-8).

(b) Gallery of Axonal morphologies and probable classifications of 8 neurons. White arrows indicate apical dendrites.

(c) Composite coronal sections show the locations of the cell body of neurons **s1-s3,** which were indicated by white arrows (EYFP signals were in green with100-μm thickness and cytoarchitectonic reference, i.e. propidium iodide (PI) signals were in red with 10-μm thickness). White dashed lines define boundary of cortical layers.

(d) Localization of the brain-wide axonal projections of neurons **s2** (dendrites: yellow; local axons: magnet; left branches and right branches originated from ipsilateral external capsule were in green and red color, respectively). The brain regions were

defined according to the Allen Brain Atlas (ABA) with the aid of the PI signals. Dashed white arrows pointed terminated directions of main axons.

Supplementary Figure 11

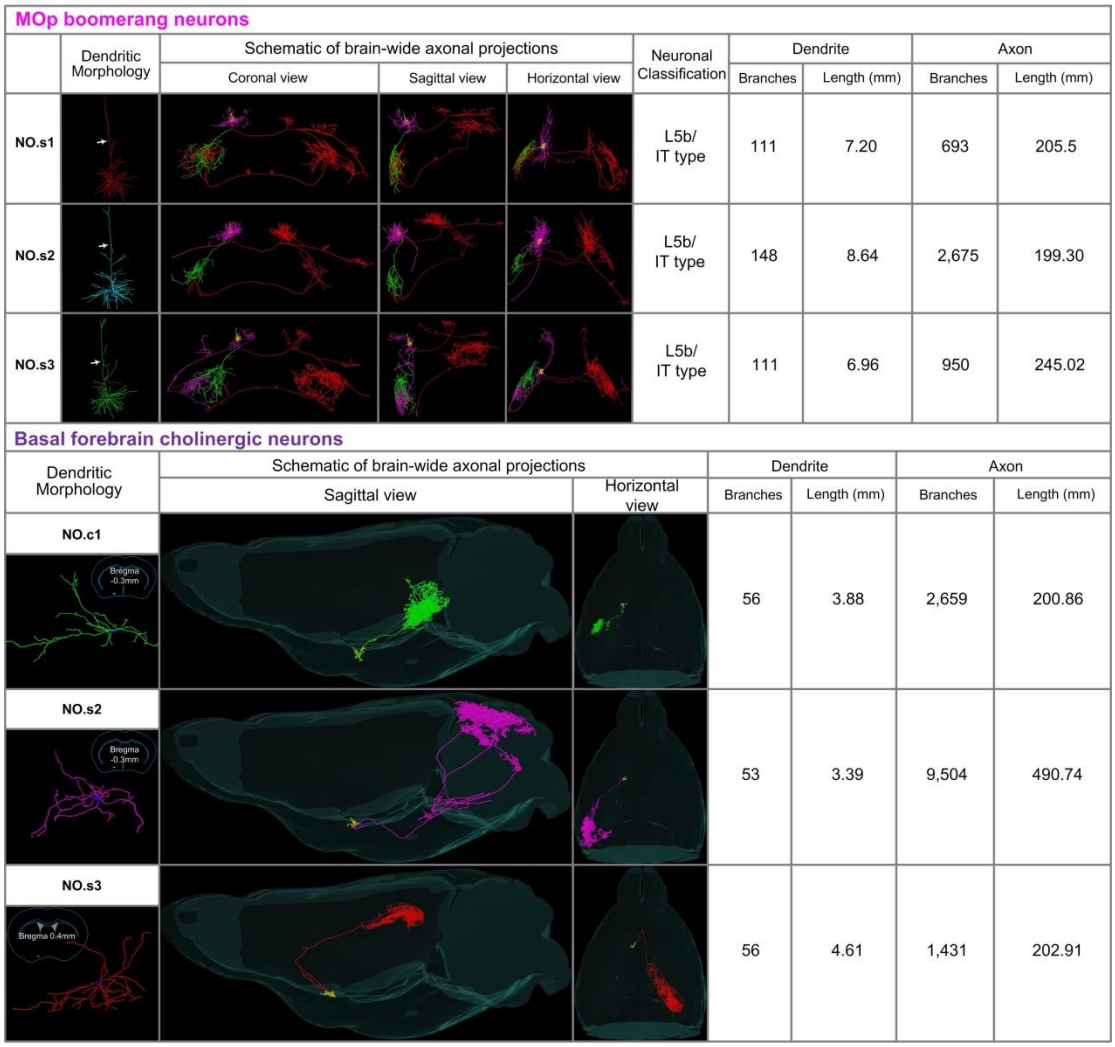

MOp boomerang neurons

	Dendritic Morphology	Schematic of brain-wide axonal projections			Neuronal Classification	Dendrite		Axon	
		Coronal view	Sagittal view	Horizontal view		Branches	Length (mm)	Branches	Length (mm)
NO.s1					L5b/ IT type	111	7.20	693	205.5
NO.s2					L5b/ IT type	148	8.64	2,675	199.30
NO.s3					L5b/ IT type	111	6.96	950	245.02

Basal forebrain cholinergic neurons

Dendritic Morphology	Schematic of brain-wide axonal projections		Dendrite		Axon	
	Sagittal view	Horizontal view	Branches	Length (mm)	Branches	Length (mm)
NO.c1			56	3.88	2,659	200.86
NO.s2			53	3.39	9,504	490.74
NO.s3			56	4.61	1,431	202.91

Supplementary figure 11

Quantitative analysis of MOp boomerang neurons (No. **s1-s3**) **and BF cholinergic neurons** (No. **c1-c3**).

For three boomerang neurons, dendrites were depicted in yellow, local axons were in magnet, left branches and right branches originated from ipsilateral external capsule were in green and red color, respectively for better differentiation. White arrows indicate apical dendrites. For three cholinergic neurons, coarse outlines and green dots indicated approximate locations of cell body, brain-wide long-range projections were demonstrated in sagittal and horizontal views, dendritic morphologies were depicted in yellow.

Supplementary Figure 12

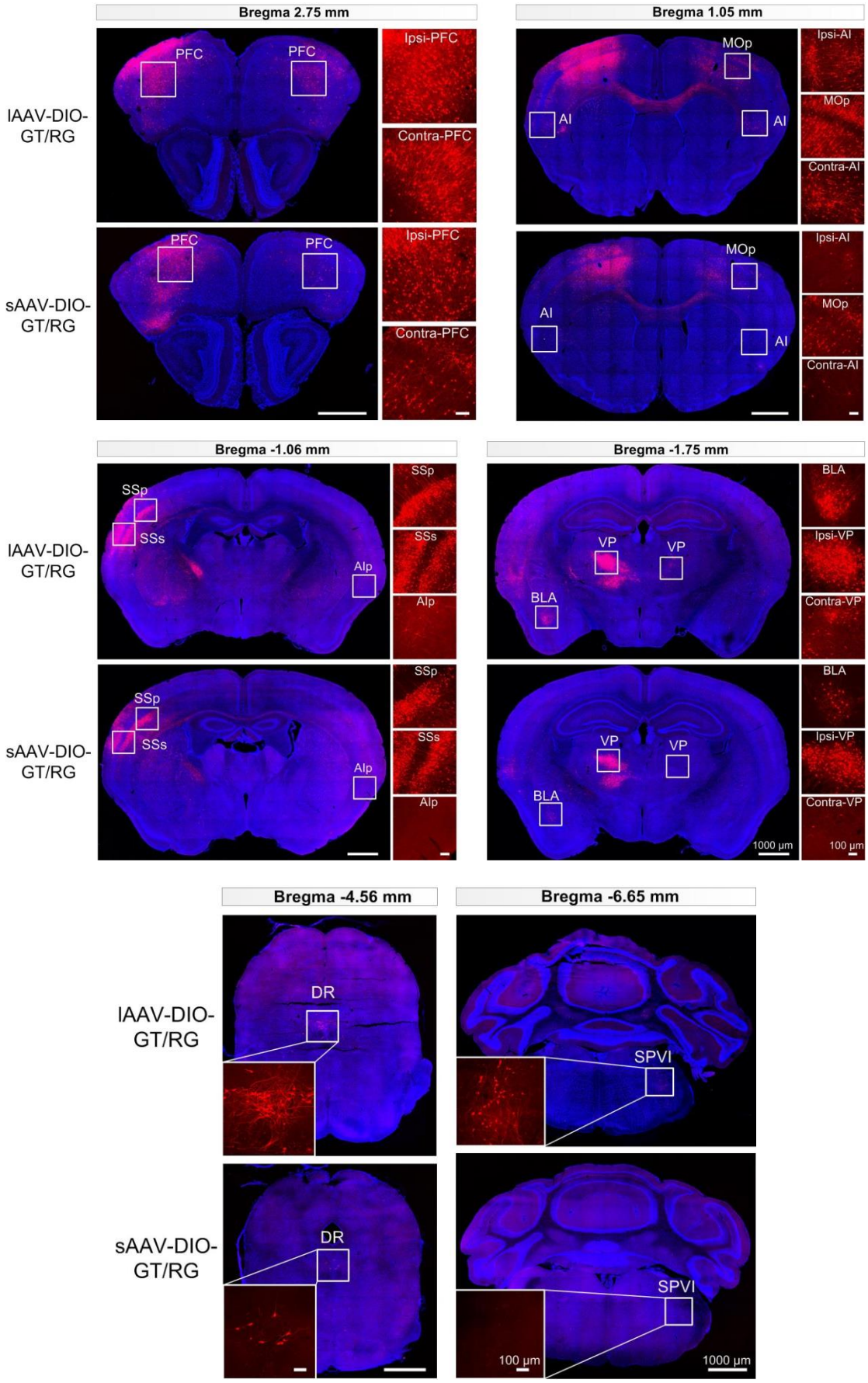

Supplementary figure 12

Localization of nuclei demonstrated in Fig. 4e with the aid of DAPI (4',6-diamidino-2-phenylindole) staining.

Abbreviations: PFC, prefrontal cortex; MOp, primary motor area; AI, agranular insular area; SSp, primary somatosensory area; SSs, supplemental somatosensory area; AIp; agranular insular area, posterior part; BLA, basolateral amygdalar nucleus; VAL, ventral anterior-lateral complex of the thalamus; VP, ventral posterior complex of the thalamus; DR, dorsal nucleus raphe; SPVI, spinal nucleus of the trigeminal, interpolar part.

Supplementary Figure 13

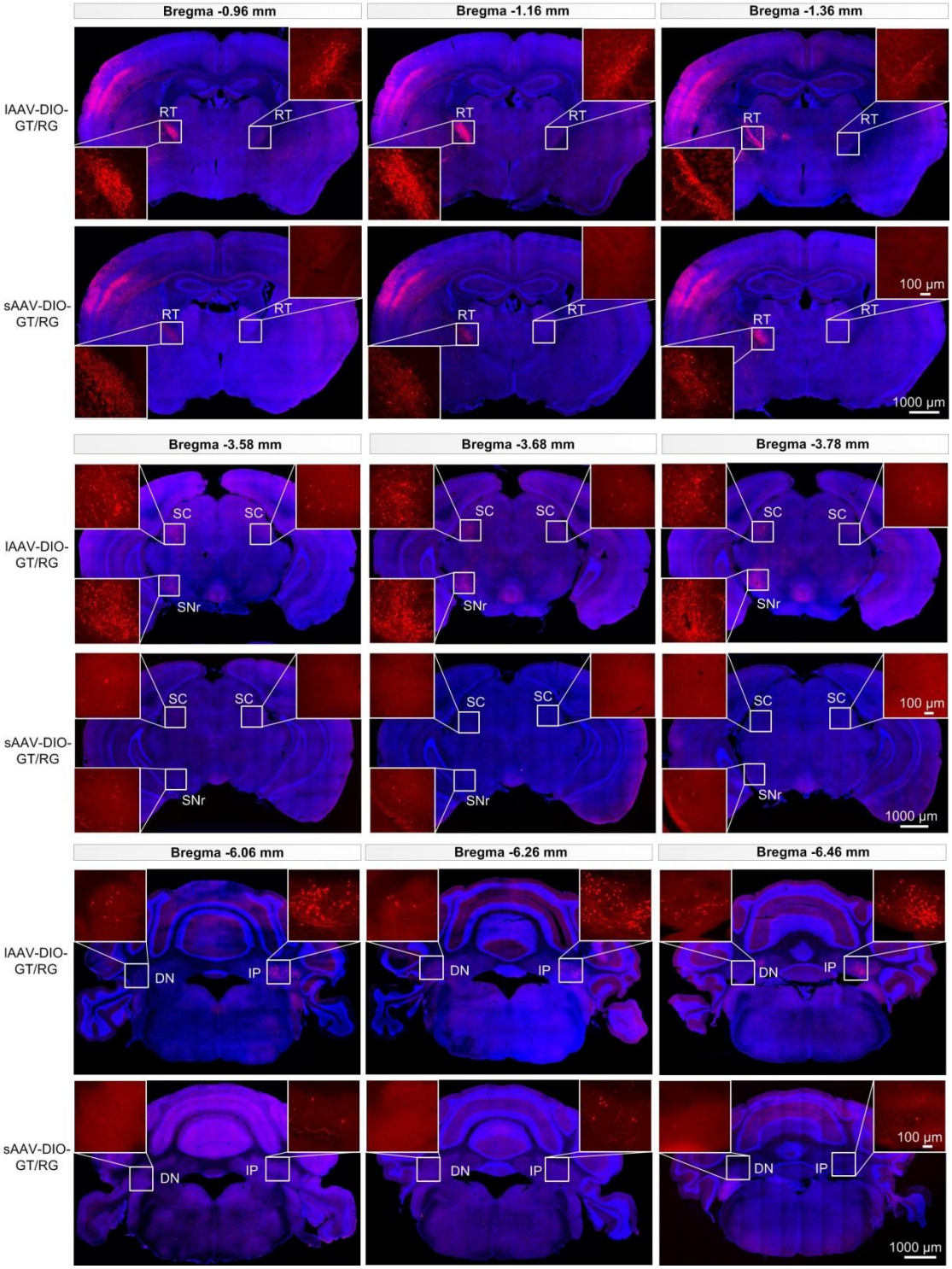

Supplementary figure 13

Comparisons of inputs in RT, SC and SNr of midbrain, DN and IP of cerebellum between lAAV-DIO-GT/RG and sAAV-DIO-GT/RG labeling groups. Insets were enlargements respective brain regions. RT, reticular nucleus of the thalamus (RT);

SC, superior colliculus; SNr, substantia nigra pars reticulate; DN, dentate nucleus; IP, interpeduncular nucleus.

Supplementary Figure 14

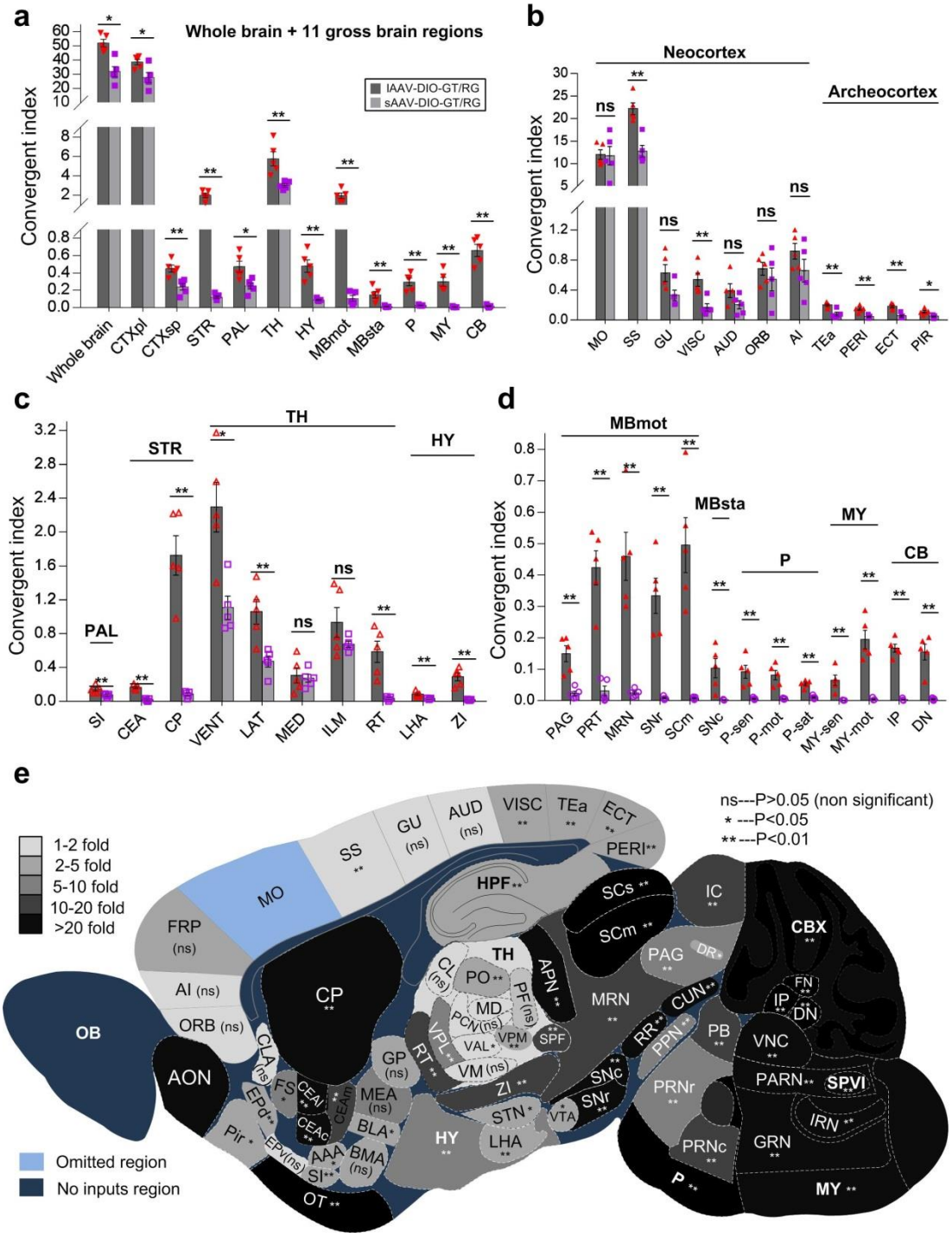

Supplementary figure 14

Brain-wide comparisons of tracing efficiency between lAAV-DIO-GT/RG and sAAV-DIO-GT/RG labeling groups.

(a) Comparisons of convergent index of total inputs and 11 gross brain regions.

(b) Comparisons of convergent index in diverse cortical regions.

(c) Comparisons of convergent index in pallidum (PAL), striatum (STR), thalamus (TH) and hypothalamus (HY).

(d) Comparisons of convergent index in midbrain, motor related (MBmot), midbrain, behavioral state related (MBsta), pons (P), medulla (MY) and cerebellum (CB).

(e) Summary of increased tracing efficiency in diverse brain regions with MAP-ENVIVDERS. All data are presented as mean ± s.e.m. n=5 mice for each group. Mann-Whitney U test. n.s, non-significant (P>0.05),*P < 0.05， **P < 0.01. Abbreviations see **Supplementary Table 2**.

Supplementary Table 1. The total numbers of labeled neurons across the whole brain after labeling with the indicated lAAVs , sAAVs and cslAAVs in different regions.

Injection site		Coordinates	Cell number across the whole brain				
			Mouse 1	Mouse 2	Mouse 3	Mouse 4	Mean ± sem
MOp	lAAV^{20,000}	AP= 1.54 ML=-1.60 DV=-1.60	652	916	688	329	646 ± 121
	lAAV^{200,000}		74	68	58	77	69 ± 4
	sAAV^{20,000}		100	182	260	236	195 ± 35
	sAAV^{40,000}		103	183	151	114	138 ± 18
	sAAV^{80,000}		66	36	16	59	44 ± 11
lAAV ^{200,000}							
CA3		AP= -1.7; ML=-2.0 DV=-2.0	49	75	59		61 ± 8
CA1		AP= -1.7; ML=-2.0 DV=-1.5	150	98	137		128 ± 16
cslAAV ^{20,000}							
Basal forebrain		AP= 0.21; ML=-1.5 DV=-5.5	46	58	48	62	54 ± 4

Supplementary Table 2. Abbreviations of anatomical structures according to the Allen Brain Atlas (ABA, http://mouse.brain-map.org/).

Abbreviations	Definitions	Abbreviations	Definitions
AAA	Anterior amygdalar area	MOBgr	Main olfactory bulb, granule layer
ac	Anterior commissure	MOBopl	Main olfactory bulb, outer plexiform layer
ACAd	Anterior cingulate area, dorsal part	MOp	Primary motor area
ACB	Nucleus accumbens	MOs	Secondary motor area
AI	Agranular insular area	MRN	Midbrain reticular nucleus
Alp	Agranular insular area, posterior part	MY	Medulla
APN	Anterior pretectal nucleus	MY-mot	Medulla, motor related
AOB	Accessory olfactory bulb	MY-sen	Medulla, sensory related
AON	Anterior olfactory nucleus	NDB	Diagonal band nucleus
AUD	Auditory areas	OB	Olfactory bulb
BLA	Basolateral amygdalar nucleus	ORB	Orbital area
BMA	Basomedial amygdalar nucleus	ORBm	Orbital area, medial part
BST	Bed nuclei of the stria terminalis	OT	Olfactory tubercle
CA1	Field CA1 of hippocampus	P	Pons
CA3	Field CA3 of hippocampus	PAG	Periaqueductal gray
CB	Cerebellum	PAL	Pallidum
CBX	Cerebellar cortex	PARN	Parvicellular reticular nucleus
cc	Corpus callosum	PB	Parabrachial nucleus
CEA	Central amygdalar nucleus	PCN	Paracentral nucleus
CEAc	Central amygdalar nucleus, capsular part	PERI	Perirhinal area
CEAl	Central amygdalar nucleus, lateral part	PF	Parafascicular nucleus
CEAm	Central amygdalar nucleus, medial part	PG	Pontine gray
CL	Central lateral nucleus of the thalamus	PIR	Piriform area
CLA	Claustrum	PL	Prelimbic area
CP	Caudoputamen	P-mot	Pons, motor related
cpd	cerebal peduncle	PO	Posterior complex of the thalamus
COAa	Cortical amygdalar area, anterior part	PPN	Pedunculopontine nucleus
CTXpl	Cortical plate	PRNc	Pontine reticular nucleus, caudal part
CTXsp	Cortical subplate	PRNr	Pontine reticular nucleus
CUN	Cuneiform nucleus	PRT	Pretectal region
df	dorsal fornix	P-sen	Pons, sensory related
DG	Dentate gyrus	py	Pyramid
DN	Dentate nucleus	RN	Red nucleus
DR	Dorsal nucleus raphe	RR	Midbrain reticular nucleus, retrorubral area
ec	external capsule	RSP	Retrosplenial area
ECT	Ectorhinal area	RT	Reticular nucleus of the thalamus
ENTm	Entorhinal area, medial part, dorsal zone	SC	Superior colliculus
Epd	Endopiriform nucleus, dorsal part	SCm	Superior colliculus, motor related
Epv	Endopiriform nucleus, ventral part	SCs	Superior colliculus, sensory related
fa	corpus callosum, anterior forceps	SI	Substantia innominata
fi	fimbria	SNc	Substantia nigra, compact part
FN	Fastigial nucleus	SNr	Substantia nigra, reticular part
FRP	Frontal pole, cerebral cortex	SPF	Subparafascicular nucleus
FS	Fundus of striatum	SPVI	Spinal nucleus of the trigeminal, interpolar part
GP	Globus pallidus	SS	Somatosensory areas
GRN	Gigantocellular reticular nucleus	SSp	Primary somatosensory area
GU	Gustatory areas	SSs	Supplemental somatosensory area
HPF	Hippocampal formation	STN	Subthalamic nucleus
HY	Hypothalamus	STR	Striatum
IC	Inferior colliculus	TEa	Temporal association areas
ILM	Intralaminar nuclei of the dorsal thalamus	TH	Thalamus
int	Internal capsule	TRS	Triangular nucleus of septum
IP	Interposed nucleus	TTd	Taenia tecta, dorsal part
IRN	Intermediate reticular nucleus	TTv	Taenia tecta, ventral part
LAT	Lateral group of the dorsal thalamus	VAL	Ventral anterior-lateral complex of the thalamus
LHA	Lateral hypothalamic area	VISC	Visceral area
LSc	Lateral septal nucleus, caudal (caudodorsal) part	VISp	Primary visual area
MBmot	Midbrain, motor related	VISl	Lateral visual area
MBsta	Midbrain, behavioral state related	VM	Ventral medial nucleus of the thalamus
MD	Mediodorsal nucleus of thalamus	VNC	Vestibular nuclei
MED	Medial group of the dorsal thalamus	VP	Ventral posterior complex of the thalamus

Supplementary Table 3. Quantifications of starter cells and total input cells of lAAV-DIO-GT/RG and sAAV-DIO-GT/RG labeling groups.

Total number of starter cells						
	Mouse 1	Mouse 2	Mouse 3	Mouse 4	Mouse 5	Mean ± sem
lAAV-DIO-GT/RG	2,999	2,308	2,396	1,940	2,286	2,386 ± 172
sAAV-DIO-GT/RG	1,842	2,406	2,155	1,974	1,817	2,039 ± 127
Total number of input cells across the whole brain						
lAAV-DIO-GT/RG	150,915	132,027	113,278	115,100	105,647	123,393 ± 9,076
sAAV-DIO-GT/RG	81,771	70,309	72,182	43,507	54,665	64,487 ± 7,617

Supplementary Table 4. Summary of viruses used in this study.

Part I----rAAVs

		Plasmids (μg/μl)	Titres (viral genome/ml)	Notes
Verification of viral interactions				
lAAV-EYFP/mCherry		A. pAAV-EF1α-EYFP (1.0 μg/μl) B. pAAV-EF1α-mCherry (0.7 μg/μl)	5.0×10^{12}	Plasmids A and B were pre-mixed at a ratio of 1:1
sAAV-EYFP/mCherry	rAAV2/9-EF1α-EYFP		5.0×10^{12}	rAAV2/9-EF1α-EYFP and rAAV2/9-EF1α-EYFP were post-mixed at a ratio of 1:1, generating sAAV-EYFP/mCherry
	rAAV2/9-EF1α-mCherry		5.0×10^{12}	
Non-cell-type-specific labelling systems (lAAVs)				
lAAVs	$lAAV^{20,000}$	A. pAAV-CMV-Cre (1.2 μg/μl); B. pAAV-EF1α-double floxed-EYFP-WPRE-HGHpA (Addgene #20296; 1.0 μg/μl)	4.0×10^{12}	Plasmids A and B were pre-mixed at a ratio of 1:20,000, 1:200,000 and 1:1,000,000, generating $lAAV^{20,000}$, $lAAV^{200,000}$ and $lAAV^{1,000,000}$, respectively
	$lAAV^{200,000}$		7.0×10^{12}	
	$lAAV^{1,000,000}$		2.9×10^{12}	
sAAVs	rAAV2/9-CMV-Cre		4.0×10^{12}	rAAV2/9-CMV-Cre and rAAV2/9-EF1α-double floxed-EYFP were post-mixed at a ratio of 1:20,000, 1:40,000, 1:80,000 and 1:1,000,000, generating $sAAV^{20,000}$, $sAAV^{40,000}$, $sAAV^{80,000}$ and $sAAV^{1,000,000}$, respectively
	rAAV2/9-EF1α-double floxed-EYFP		1.0×10^{13}	
Cell-type-specific labelling systems (cslAAVs)				
cslAAVs	$cslAAV^{2,000}$	A. pAAV-EF1α-Flp (1.0 μg/μl); B. pAAV-hSyn Con/Fon EYFP (Addgene #55650; 1.0 μg/μl)	7.1×10^{12}	Plasmids A and B were pre-mixed at a ratio of 1:2,000 and 1:20,000, generating $cslAAV^{2,000}$ and $cslAAV^{20,000}$, respectively
	$cslAAV^{20,000}$		7.0×10^{12}	
cssAAVs	rAAV2/9-EF1α-Flp		2.0×10^{12}	rAAV2/9-EF1α-Flp and rAAV2/9-hSyn Con/Fon EYFP were post-mixed at a ratio of 1:2,000 and 1:20,000, generating $cssAAV^{2,000}$ and $cssAAV^{20,000}$, respectively
	rAAV2/9-hSyn Con/Fon EYFP		5.0×10^{12}	
Monosyanptic tracing systems				
lAAV-DIO-GT/RG		A. pAAV-EF1α-DIO-EGFP-TVA (GT) (1.0 μg/μl) B. pAAV-EF1α-DIO-RG (0.5 μg/μl)	7.0×10^{12}	Plasmids A and B were pre-mixed at a ratio of 1:2
sAAV-DIO-GT/RG	rAAV2/9-EF1α-DIO-EGFP-TVA		5.6×10^{12}	rAAV2/9-EF1α-DIO-EGFP-TVA and rAAV2/9-EF1α-DIO-RG were post-mixed at a ratio of 1:2, generating sAAV-DIO-GT/RG
	rAAV2/9-EF1α-DIO-RG		6.3×10^{12}	

Part II----RV

EnvA-SADΔG-DsRed	Titre: 2.0×10^{8} infectious particles/ml